



ELSEVIER

Available online at www.sciencedirect.com

SCIENCE @ DIRECT®

Journal of volcanology
and geothermal research

Journal of Volcanology and Geothermal Research 127 (2003) 269–303

www.elsevier.com/locate/jvolgeores

Water-level changes induced by local and distant earthquakes at Long Valley caldera, California

Evelyn Roeloffs^{a,*}, Michelle Sneed^b, Devin L. Galloway^b, Michael L. Sorey^c,
Christopher D. Farrar^d, James F. Howle^d, Jennifer Hughes^e

^a U.S. Geological Survey, 1300 SE Cardinal Court, Vancouver, WA 98683, USA

^b U.S. Geological Survey, Sacramento, CA 95819, USA

^c U.S. Geological Survey, Retired, Portola Valley, CA 94028, USA

^d U.S. Geological Survey, Carnelian Bay, CA 96140, USA

^e 808 21st St., Apt. 233, Bellingham, WA 98225, USA

Accepted 19 March 2003

Abstract

Distant as well as local earthquakes have induced groundwater-level changes persisting for days to weeks at Long Valley caldera, California. Four wells open to formations as deep as 300 m have responded to 16 earthquakes, and responses to two earthquakes in the 3-km-deep Long Valley Exploratory Well (LVEW) show that these changes are not limited to weathered or unconsolidated near-surface rocks. All five wells exhibit water-level variations in response to earth tides, indicating they can be used as low-resolution strainmeters. Earthquakes induce gradual water-level changes that increase in amplitude for as long as 30 days, then return more slowly to pre-earthquake levels. The gradual water-level changes are always drops at wells LKT, LVEW, and CH-10B, and always rises at well CW-3. At a dilatometer just outside the caldera, earthquake-induced strain responses consist of either a step followed by a contractional strain-rate increase, or a transient contractional signal that reaches a maximum in about seven days and then returns toward the pre-earthquake value. The sizes of the gradual water-level changes generally increase with earthquake magnitude and decrease with hypocentral distance. Local earthquakes in Long Valley produce coseismic water-level steps; otherwise the responses to local earthquakes and distant earthquakes are indistinguishable. In particular, water-level and strain changes in Long Valley following the 1992 M7.3 Landers earthquake, 450 km distant, closely resemble those initiated by a M4.9 local earthquake on November 22, 1997, during a seismic swarm with features indicative of fluid involvement. At the LKT well, many of the response time histories are identical for 20 days after each earthquake, and can be matched by a theoretical solution giving the pore pressure as a function of time due to diffusion of a nearby, instantaneous, pressure drop. Such pressure drops could be produced by accelerated inflation of the resurgent dome by amounts too small to be detected by the two-color electronic distance-measuring network. Opening-mode displacement in the south moat, inferred to have followed a M4.9 earthquake on November 22, 1997, could also create extensional strain on the dome and lead to water-level changes similar to those following dome inflation. Contractional strain that could account for earthquake-induced water-level rises at the CW-3 well is inconsistent with geodetic observations. We instead attribute these water-level rises to diffusion of elevated fluid pressure localized in the south moat thermal aquifer. For hydraulic diffusivities appropriate to the upper few hundred

* Corresponding author. Tel.: +1-360-9938937; Fax: +1-360-9938980.

E-mail address: evelynr@usgs.gov (E. Roeloffs).

meters at Long Valley, an influx of material at temperatures of 300°C can thermally generate pressure of 6 m of water or more, an order of magnitude larger than needed to account for the CW-3 water-level rises. If magma or hot aqueous fluid rises to within 1 km of the surface in the eastern part of the south moat, then hydraulic diffusivities are high enough to allow fluid pressure to propagate to CW-3 on the time scale observed. The data indicate that seismic waves from large distant earthquakes can stimulate upward movement of fluid in the hydrothermal system at Long Valley.

© 2003 Elsevier B.V. All rights reserved.

Keywords: volcanoes; Long Valley caldera; earthquakes; hydrothermal systems

1. Introduction

Groundwater levels in wells, and discharges at several springs and creeks, have been monitored since the early 1980's at Long Valley caldera, a hazardous volcanic area in eastern California (Fig. 1). Tectonic activity at Long Valley is also monitored by a seismic network, periodic leveling surveys, a two-color electronic distance-measuring (EDM) network, three borehole volumetric strainmeters (dilatometers), a long-baseline tiltmeter, and, more recently, survey-mode and continuous GPS. Earthquake swarms and episodes of accelerated deformation are interpreted as periods of heightened hazard (Hill et al., 2002).

The purposes of the hydrologic monitoring are to characterize the groundwater flow and hydrothermal regimes and to evaluate whether fluid-pressure or discharge changes contain useful information about the volcano's state. Five wells that are monitored with transducers exhibit groundwater-level fluctuations in response to earth tides, indicating that they respond to crustal strain.

Groundwater levels at Long Valley change in response to local seismicity as well as large earthquakes up to several hundred kilometers away. More specifically, local earthquakes produce immediate (within 15 min) water-level steps that can be approximately accounted for as poroelastic responses to coseismic static strain. Although distant earthquakes do not produce steps, both local and distant earthquakes initiate gradual water-level changes that increase in amplitude for several weeks and return to pre-earthquake values only after several months. The process causing these gradual post-earthquake water-level changes appears to be initiated by seismic waves.

Long-lasting water-level offsets induced by seismic waves from distant earthquakes have been studied at several locations (Matsumoto, 1992; Roeloffs, 1998; Brodsky et al., 2002). Only certain wells exhibit this phenomenon, which has several distinctive features. At each responding well, water level either always rises or always falls, regardless of the location or focal mechanism of the earthquake. The time histories of the water-level changes closely match the calculated responses to step-like water pressure changes occurring near, but not at, the well site. Possible mechanisms for these changes include a liquefaction-like increase in fluid pressure (for shallow wells) (Roeloffs, 1998), escape of gas bubbles from the aquifer (Matsumoto and Roeloffs, 2003), or permeability changes due to unclogging of narrow fractures (Brodsky et al., 2002). All of these mechanisms can operate in well-aquifer systems in tectonically quiet locations. In contrast, we show here that the earthquake-induced water-level changes at Long Valley, considered with seismicity and other crustal deformation data, actually reflect accelerated deformation, accompanied by upward movement of magma or hot aqueous fluid at elevated temperatures beneath the caldera south moat.

2. Tectonic setting, instrumentation, and data

Fig. 2 shows the locations of hydrologic monitoring sites, borehole strainmeters (dilatometers), and the most frequently surveyed portion of the two-color EDM network, together with major tectonic features at Long Valley. The resurgent dome is a topographic high which began to rise after the caldera-forming eruption about 760 000 years ago (Bailey, 1989). Since 1980, leveling campaigns and

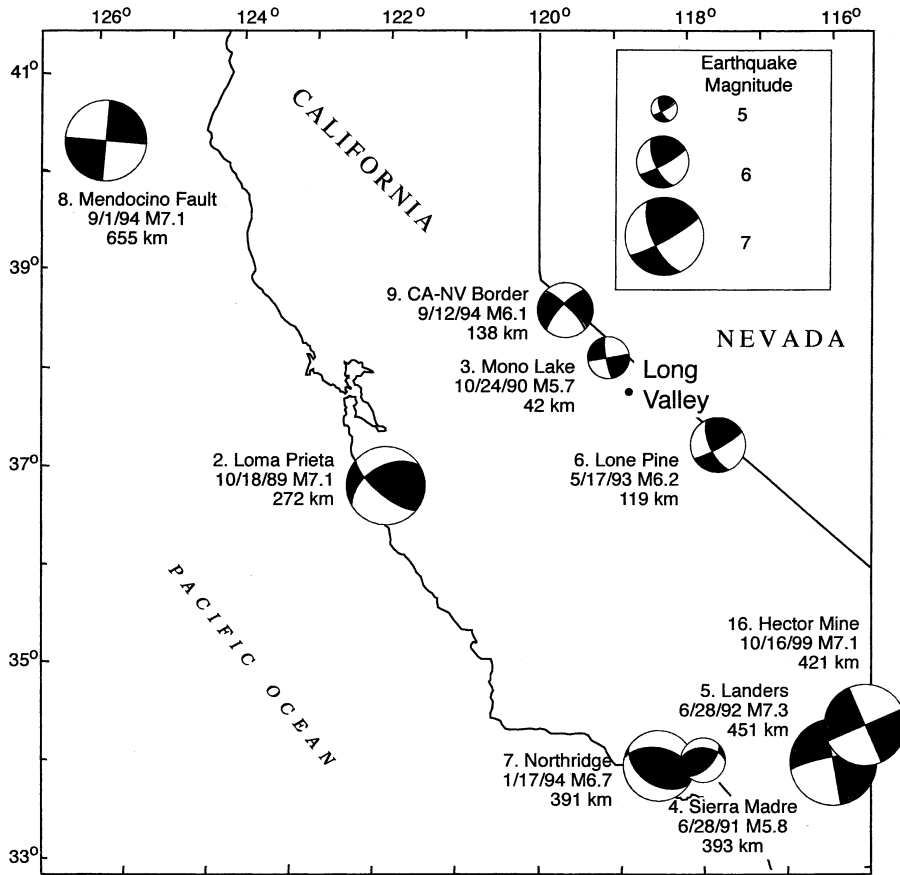


Fig. 1. Map of California showing locations of Long Valley and of nine earthquakes outside the Long Valley area that produced water-level changes. Event numbers correspond to Table 3 and Fig. 4a.

measurements by the two-color EDM network have recorded more than 0.7 m of dome uplift, with accelerated episodes in 1980, 1983, 1989 and 1997 (Bailey and Hill, 1990; Hill et al., 2002). Uplift of the resurgent dome dominates deformation at Long Valley, and has been attributed to inflation of a spherical or ellipsoidal source 6 to 8 km beneath the dome (Langbein et al., 1993; Langbein et al., 1995; Langbein, 2003 – this issue). Episodes of rapid dome uplift have been accompanied by intensified seismicity, near Mammoth Mountain in 1989 and in the caldera south moat in 1997. The Hilton Creek fault, which is the eastern Sierra range-front fault, extends into the eastern part of the caldera south moat (Fig. 2). In 1998 and 1999, several moderate earth-

quakes occurred west of the Hilton Creek fault, near epicenters of major earthquakes in May, 1980 (Prejean et al., 2002).

Within the caldera, surficial rocks include post-caldera basalt flows, rhyolite flows, and tuffs, as well as fluvial and lacustrine sediments. These rocks overlie a welded section of the Bishop Tuff, which was erupted during the caldera-forming eruption (Bailey, 1989). The Long Valley Exploratory Well (LVEW) penetrates through the Bishop Tuff 2.2 km beneath the surface into pre-caldera metamorphic rocks (McConnell et al., 1995). The other continuously monitored wells are completed in either post-caldera rocks or the Bishop Tuff.

The caldera west, south, and east moats contain

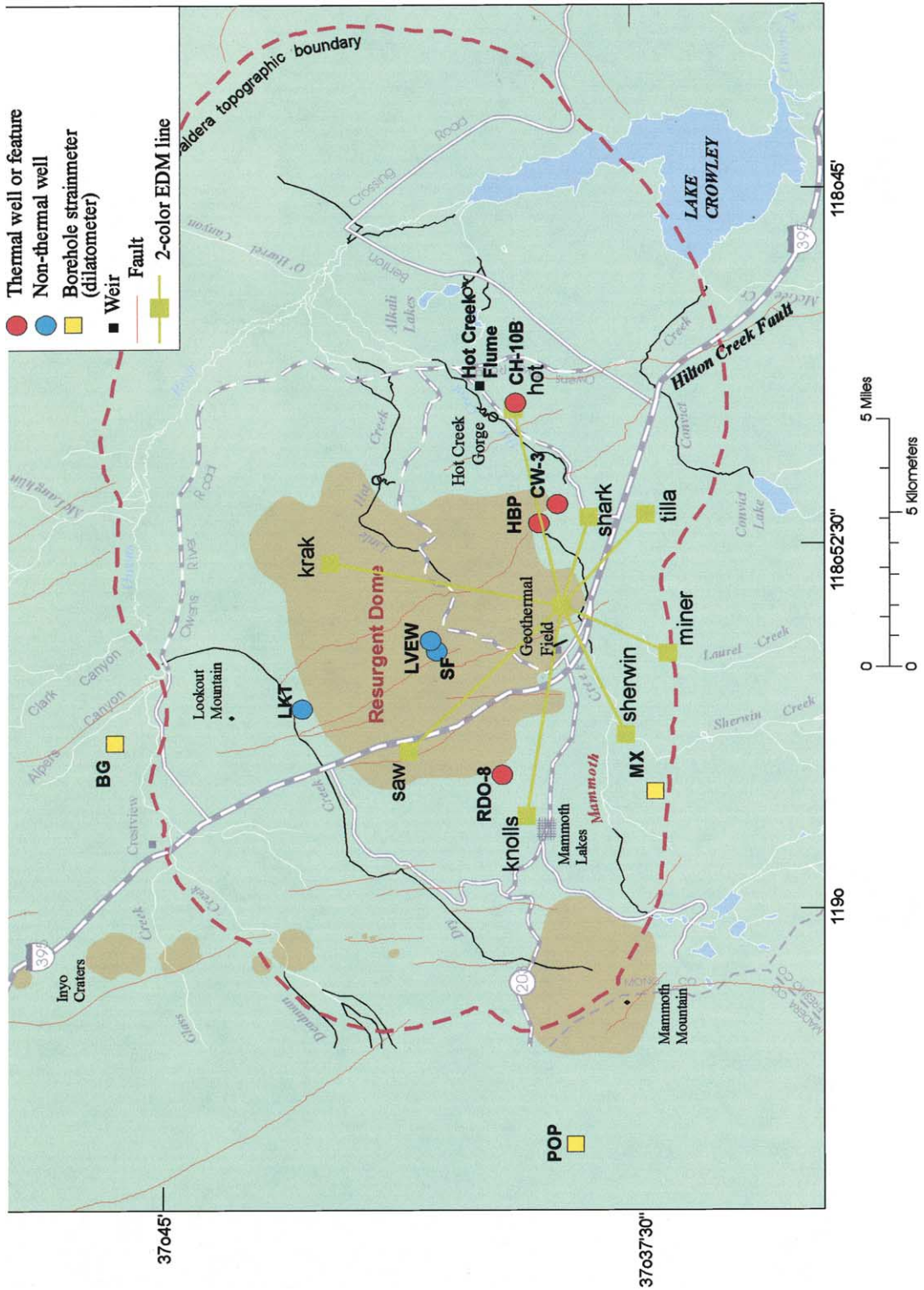


Fig. 2. Map of the Long Valley area showing observation wells, strainmeters, and the two-color EDM network.

an active hydrothermal system. The existence of one or more relatively high-permeability thermal aquifers in the upper 1000 m is indicated by temperature maxima in this depth range in many thermal wells. The boreholes that have encountered the hottest water (200–220°C) are in the caldera west moat, suggesting that the present-day heat source is related to recent Mono-Inyo volcanism (Sorey, 1985; Sorey et al., 1991). Thermal water flows generally from west to east to discharge along fault zones in the south and east moats.

2.1. Hydrologic data

The analysis here is based on data from five wells within the caldera where groundwater levels have been monitored at frequent intervals and are currently recorded using transducers (Howle and Farrar, 1996). Fig. 3 shows completion diagrams for each well. Automated groundwater-level measurements are supplemented by manual measurements, typically accurate to 0.3 cm, made several

times per year to check for transducer drift. Two of the wells, CW-3 and CH-10B, are hot-water wells completed in the eastern part of the thermal aquifer. LKT and SF are non-thermal wells. The LVEW is 3 km deep with a maximum temperature of 100°C, and is not considered to be a thermal well. Fig. 4a shows the daily average water levels from 1985 through July, 1999, for CW-3, CH-10B, LKT, and SF; only intermittent data are available for LVEW and they are shown in Section 3.

Annual precipitation averaged 682 mm/year from 1982 through 1998 (Fig. 4b), with typically half falling from November through March as snow. Most infiltration presumably occurs after snow begins to melt in March.

Although water-level changes induced by earthquakes are visible in the long-term hydrographs (Fig. 4a; Table 1), variations in recharge due to precipitation are the most prominent features. LKT has the most pronounced seasonal response, and above-average precipitation in 1982 and 1983 probably accounts for the elevated water levels

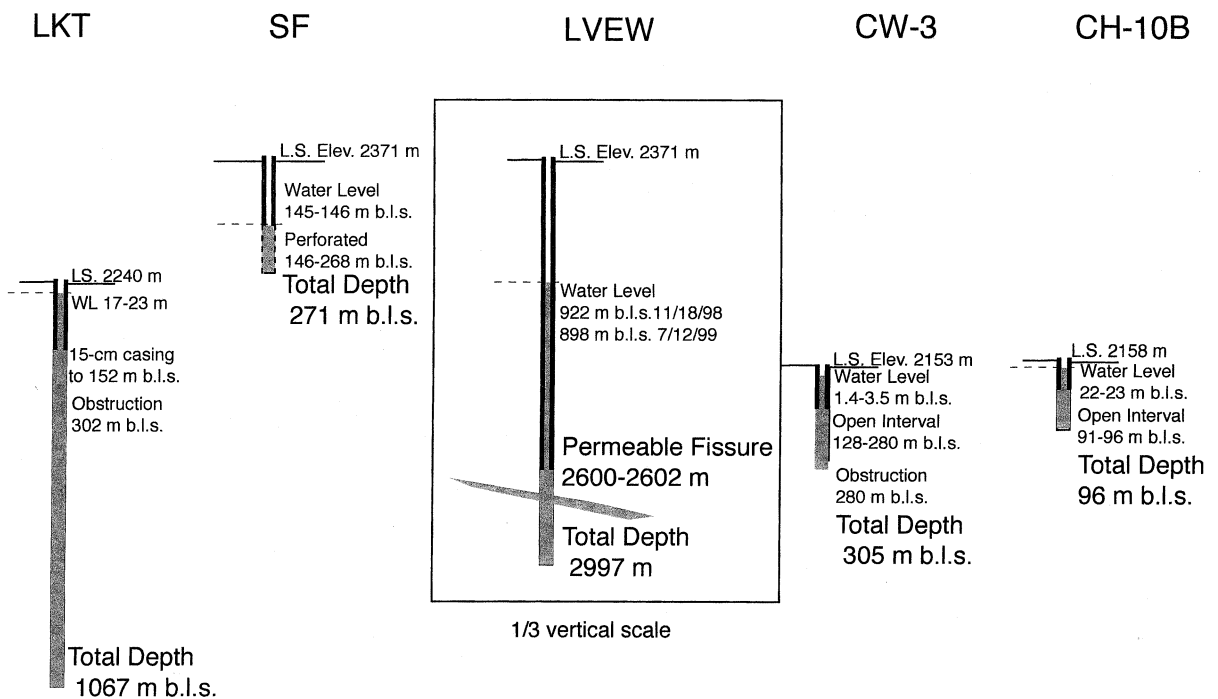


Fig. 3. Diagrams of well completions (L.S., land surface; m b.i.s., meters below ground surface).

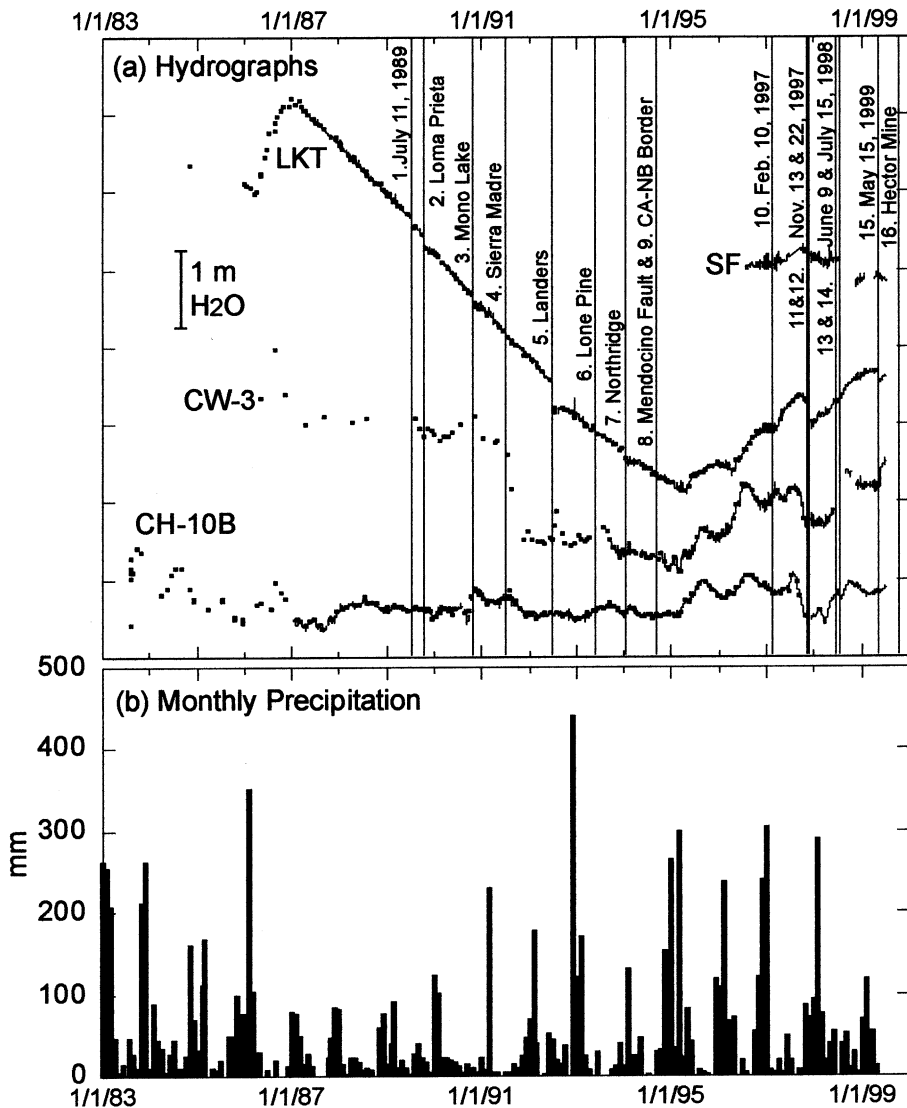


Fig. 4. (a) Daily average water levels in CH-10B, CW-3, LKT, and SF. Manual measurements are superimposed for CH-10B, CW-3, and LKT. The times of 16 earthquakes that produced water-level changes are indicated. (b) Monthly precipitation calculated from daily observations at the Mammoth Lakes Ranger Station.

there at the beginning of monitoring. The 1986 groundwater-level rises in LKT, CW-3 and CH-10B also appear to be caused by substantial precipitation. During low-precipitation years from 1987 to 1994, water level at LKT fell steadily. Annual spring groundwater-level rises of 0.5–1 m in LKT and CW-3 resumed with consistently above-average precipitation 1995 through 1998. The 1-m de-

cline in water level in CW-3 during 1991 has been attributed to pressure declines in the geothermal aquifer at Casa Diablo associated with tripling of the production rate (Sorey and Farrar, 1998).

2.2. Borehole strain data

Crustal deformation sensors with earth tidal

Table 1
Earthquakes that caused gradual water-level responses in the LKT well

Event No.	Date	Time (UT)	Location or Name	Latitude (°N)	Longitude (°W)	Depth (km)	Magnitude	Distance from LKT (km)
1	July 11, 1989	04:13	Long Vally	37.418	118.642	12	4.6 ^a	42
2	Oct. 18, 1989	00:04	Loma Prieta	37.036	121.883	18	7.1 ^b	272
3	Oct. 24, 1990	06:15	Mono Lake	38.047	119.157	12	5.7 ^a	42
4	June 28, 1991	14:44	Sierra Madre	34.262	118.002	11	5.8 ^c	393
5	June 28, 1992	11:57	Landers	34.201	116.436	1	7.3 ^c	451
6	May 17, 1993	23:20	Lone Pine	37.171	117.775	6	6.2 ^d	119
7	Jan. 17, 1994	12:31	Northridge	34.213	118.537	18	6.7 ^c	391
8	Sept. 1, 1994	15:16	Mendocino Flt.	40.402	125.68	10	7.1 ^c	655
9	Sept. 12, 1994	12:24	CA-NV Border	38.819	119.652	14	6.1 ^c	138
10	Feb. 10, 1997	23:26	Long Valley	37.565	118.861	9	4.2 ^e	17.9
11	Nov. 13, 1997	19:42	Long Valley	37.646	118.899	6	4.1 ^a	8.3
12	Nov. 22, 1997	17:20	Long Valley	37.638	118.934	7	4.9 ^c	8.7
13	June 9, 1998	05:25	Long Valley	37.589	118.7953	6.7	5.2 ^a	18.4
14	July 15, 1998	04:53	Long Valley	37.563	118.806	6.2	5.1 ^c	20.2
15	May 15, 1999	13:22	Long Valley	37.530	118.817	5.0	5.6 ^c	23.0
16	Oct. 16, 1999	09:46	Hector Mine	34.594	116.271	16	7.1 ^c	421

^a Local magnitude.

^b Surface wave magnitude.

^c Moment magnitude.

^d Duration magnitude.

resolution include a borehole strainmeter (dilatometer) at 162 m depth west of Mammoth Mountain (POP in Fig. 2) (Johnston et al., 1995). The original POP strainmeter failed in July, 1995 and was replaced in September, 1995. Two additional dilatometers, MX (164 m deep) and BG (165 m deep), were installed in 1999.

Raw dilatometer data, sampled every 10 min, are expressed in terms of volumetric strain by determining the amplitude of the M_2 earth tide constituent (frequency of 1.9322736 cpd) in unscaled counts and equating it to the calculated amplitude of M_2 , 10.2×10^{-9} . The calculated amplitude was obtained using the program GOTIC II (Matsumoto et al., 2000; Sato and Hanada, 1984) and assumes an elastic earth with ocean loading. The strain induced by atmospheric pressure fluctuations can be removed from the data using a coefficient determined by linear regression.

The POP strain data exhibit a seasonal response averaging 2×10^{-6} peak-to-peak each year which proves difficult to remove. Our interest here is primarily in shorter-term signals, so the strain data shown in later plots are corrected

only for linear trends in the time periods immediately prior to earthquakes.

2.3. Tidal and barometric response of groundwater levels

Water levels in wells respond to crustal strain induced by both earth tides and atmospheric pressure variations. Earth-tide-induced fluctuations establish that water levels respond to crustal strain, and allow water-level changes to be expressed in units of strain. Atmospheric pressure acting on the ground surface, water table, and well water surface causes water levels to vary in approximate inverse proportion to atmospheric pressure variations, although the well response can be frequency dependent.

Analysis of tidally induced water-level fluctuations yields coefficients of proportionality between groundwater-level change and crustal strain (see, for example, Roeloffs (1996)). More specifically, the M_2 (1.9322736 cpd) and O_1 (0.9295357 cpd) tidal frequencies can be isolated in the water-level data, and compared in amplitude and phase to theoretical tidal variations, and/or to the same

frequencies in dilatometer data. In an ideal, perfectly confined porous formation, both frequencies would be in phase with borehole strain, or calculated tidal strain, and the same coefficient of proportionality would hold for both M_2 and O_1 . This coefficient represents the fluid-pressure change, Δp , caused by an increment of volumetric strain, $\Delta \varepsilon_{kk}$, under undrained conditions and is given by:

$$\Delta p = BK_u \Delta \varepsilon_{kk} \quad (1)$$

where B is Skempton's coefficient and K_u is the undrained bulk modulus (e.g. Roeloffs, 1996). For many well-aquifer systems, the effects of fluid flow cause the tidal fluctuations of well water level to lag or lead tidally induced fluid-pressure variations in the formation. In such cases, the ratios of water-level tides to strain tides must be corrected to obtain BK_u .

Table 2 lists the tidal responses of water levels in the wells and derived strain sensitivities, BK_u , based on the analysis by Galloway et al. (1999). LVEW is now known to have the largest strain sensitivity, but the earthquake-induced signals were recorded at times when the borehole conditions or sensor limitations prevented the recording of tidal fluctuations. Of the shallower wells, LKT is the most sensitive to strain ($BK_u = 0.495 \text{ m}/10^{-6}$) and CH-10B is the least sensitive. At CW-3, there are large phase lags of the M_2 and O_1 constituents relative to the theoretical earth tide which Galloway et al. (1999) interpret to indicate wellbore storage, concluding that the apparent strain sensitivity determined from M_2 amplitudes is only about 60% of BK_u . Wellbore storage is

negligible at sufficiently low frequencies, but because the signals we are evaluating here span frequencies both higher and lower than the tidal frequencies, we ascribe a large error bar to the CW-3 strain sensitivity.

2.4. Aquifer parameters

Hydraulic diffusivity, c , governs the time scale over which strain-induced fluid-pressure changes dissipate:

$$c = K/S_s \quad (2)$$

where K is hydraulic conductivity, and S_s is specific storage. The specific storage is in turn given by:

$$S_s = \rho_f g (\beta + \phi \beta_f) \quad (3)$$

where ρ_f is fluid density, g is acceleration due to gravity, β is the vertical compressibility of the porous medium, ϕ is porosity, and β_f is the compressibility of the fluid (0.435 GPa^{-1} for water at 20°C).

Sorey et al. (1978) give porosities and permeabilities from borehole cores in Long Valley that can be used to infer specific storages and hydraulic diffusivities (Fig. 5a). The highest diffusivities are in unaltered sediments and tuffs; hydrothermally altered rocks and flow rocks have the lowest diffusivities.

For LKT, a slug test yielded horizontal hydraulic conductivity of $2 \times 10^{-4} \text{ m s}^{-1}$ (Rojstaczer, 1988) and analysis of the tidal and barometric responses yielded $S_s = 1.7\text{--}2 \times 10^{-6} \text{ m}^{-1}$ (Rojstaczer and Agnew, 1989), implying a high horizontal hydraulic diffusivity of $100\text{--}117 \text{ m}^2 \text{ s}^{-1}$. Rojstaczer (1988) also estimated a maximum vertical hydraulic conductivity of $7 \times 10^{-9} \text{ m s}^{-1}$ for LKT, corresponding to a vertical hydraulic diffusivity of $0.003 \text{ m}^2 \text{ s}^{-1}$.

Transmissivity of the geothermal field (Fig. 2), based on pre-production gradients as well as later production data, is approximately $0.005 \text{ m}^2 \text{ s}^{-1}$, corresponding to a hydraulic conductivity of $2.4 \times 10^{-5} \text{ m s}^{-1}$ for a thickness of 200 m; if storativities are comparable to other caldera rocks

Table 2
Tidal response coefficients of wells

Well	Volumetric strain sensitivity (m/ppm, M_2)	Volumetric strain sensitivity (m/ppm, O_1)
CH-10B	0.039 ± 0.024	0.000
CW-3	0.250 ± 0.053	0.000
LKT	0.495 ± 0.080	0.435 ± 0.147
LVEW	2.47 ± 0.65	2.58 ± 1.06
SF	0.129 ± 0.047	0.000

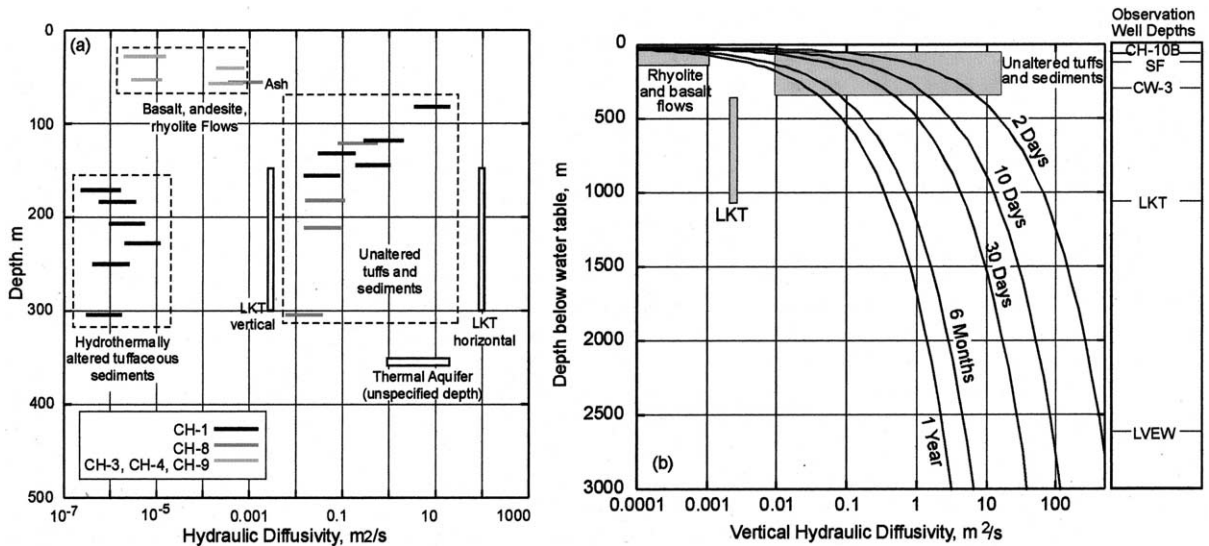


Fig. 5. (a) Diffusivities for materials in Long Valley caldera. Values for CH-1, -3, -4, -8, and -9 were calculated from measured porosities and vertical permeabilities given by Sorey et al. (1978), assuming compressibility β in the range 0.02–0.2 GPa⁻¹ for rocks with porosities less than 15% and $\beta=0.2$ to 2 GPa⁻¹ for rocks with porosities > 30%. Values for LKT are from Rojstaczer (1988), and the thermal aquifer value is an average of values obtained by various techniques. (b) Influence of diffusivity and observation well depth on time period for which a strain-induced pressure step can be sustained.

(10⁻⁶–2 × 10⁻⁵ m⁻¹) then hydraulic diffusivities, c , range from 1 to 24 m² s⁻¹.

The overall picture is one of geologic units with high diffusivities (0.1–100 m² s⁻¹) interbedded with or overlain by rocks of diffusivity as low as 3 × 10⁻⁴ m² s⁻¹. Such layering can create well-confined aquifers in which horizontal flow takes place rapidly.

The time period, τ , over which a pressure disturbance induced by aquifer strain is reduced to one-tenth of its peak amplitude by vertical flow to the water table is:

$$\tau = 11z_w^2/c \quad (4)$$

where z_w is the depth below the water table (Roeloffs, 1996). At LKT, the low vertical diffusivity and relatively great depth imply that vertical flow would not dissipate strain-induced fluid-pressure changes for a period of a year or more; as will be shown in Section 5, dissipation by horizontal flow apparently takes place more quickly. For the LVEW, strain-induced pressure changes also can be expected to be unaffected by vertical flow for periods of years. The other observation wells are

relatively shallow and would not be expected to sustain strain-induced pressure changes for more than a few days unless they penetrate layers of flow rocks or hydrothermally altered materials. In particular, the water-level response to earthquakes in well SF dissipates rapidly, suggesting it is poorly confined.

3. Earthquake-related water-level and strain changes

A general earthquake-induced water-level response at Long Valley consists of an abrupt coseismic step (for local earthquakes), followed by a gradual water-level change that increases in amplitude for a period of time, then returns more slowly to the pre-earthquake level. Typical earthquake-induced strain responses at POP consist of a coseismic step followed either by a contractional increase in strain rate or by a transient contractional signal that reaches a maximum and then returns to the pre-earthquake value. The sizes of the steps and subsequent gradual changes are listed in Table 3.

Table 3
SIZES of water-level and strain changes

Event number	Earthquake Date and Time (UT)	CH-10B gradual water-level change (m)	CW-3 step water-level change (m)	CW-3 gradual water-level change (m)	LKT step water-level change (m)	LKT gradual water-level change (m)	POPA step-like change (ppm)	POPA transient change (ppm)	POPA rate change?
1	July 11, 1989	0	no data	no data	0	−0.070	0		
2	Oct. 18, 1989	0	no data	no data	0	−0.146	−0.133 ^a		yes
3	Oct. 24, 1990	0	no data	no data	0	−0.126	0		yes
4	June 28, 1991	−0.024 ± 0.01	no data	no data	0	−0.044	0		
5	June 28, 1992	−0.07	0	0.35	0	−0.396 ^b	0	−0.258	
6	May 17, 1993	0	no data	no data	0	−0.085	0		
7	Jan. 17, 1994	0	0	0.045 ± 0.080	0	−0.128	−0.063 ^a		yes
8	Sept. 1, 1994	0	no data	no data	0	−0.030	−0.011 ^a		
9	Sept. 12, 1994	0	no data	no data	0	−0.039	0		
10	Feb. 10, 1997	0	0	0.125	0	−0.056	0		
11	Nov. 13, 1997	0	0	0.03	0	−0.070	0		
12	Nov. 22, 1997, 17:20	0	−0.05	0.44 ± 0.10	0.014	−0.157	0.017	−0.370	
13	June 9, 1998	0	0	0.3	0	−0.115	0		
14	July 15, 1998	−0.034 ± 0.005	no data	no data	0	−0.039	0		
15	May 15, 1999	−0.064	−0.072	0.42	−0.032	−0.162	0.022		
16	Oct. 16, 1999	0	0	0.12	0	−0.170	−0.060 ^a		yes

Uncertainties in water-level changes are ±0.003 m unless otherwise noted. Uncertainties in strain changes are 0.005 ppm.

^a These strain steps are not consistent with coseismic static strain.

^b Estimated from manual readings after transducer failure.

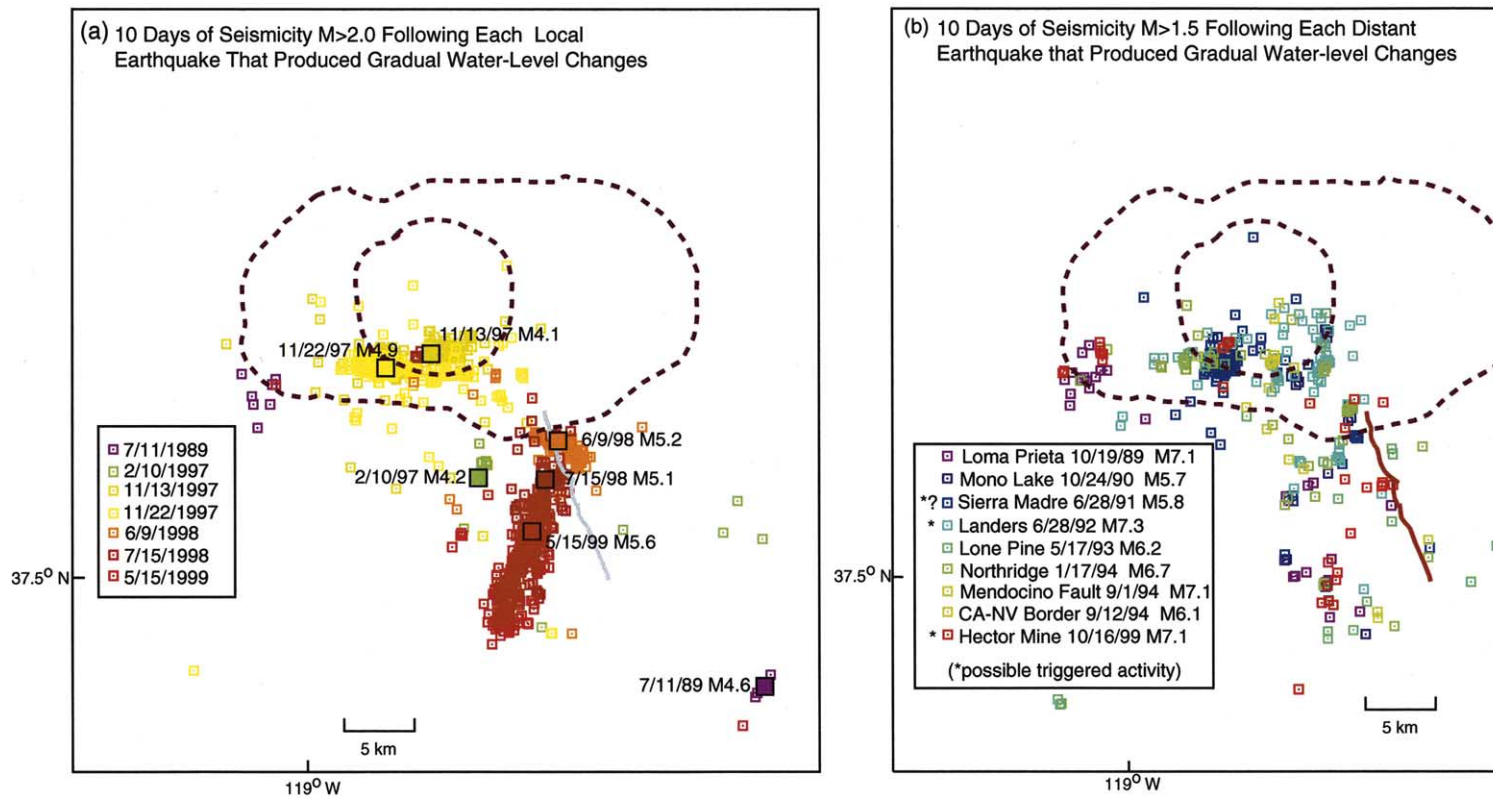


Fig. 6. (a) Earthquakes $M > 2.0$ in the Northern California Earthquake Data Center (NCEDC) catalog for 10 days following each earthquake listed in Table 3 that occurred within Long Valley caldera. (b) Earthquakes $M > 1.5$ for 10 days following each earthquake in Table 3 outside of Long Valley caldera.

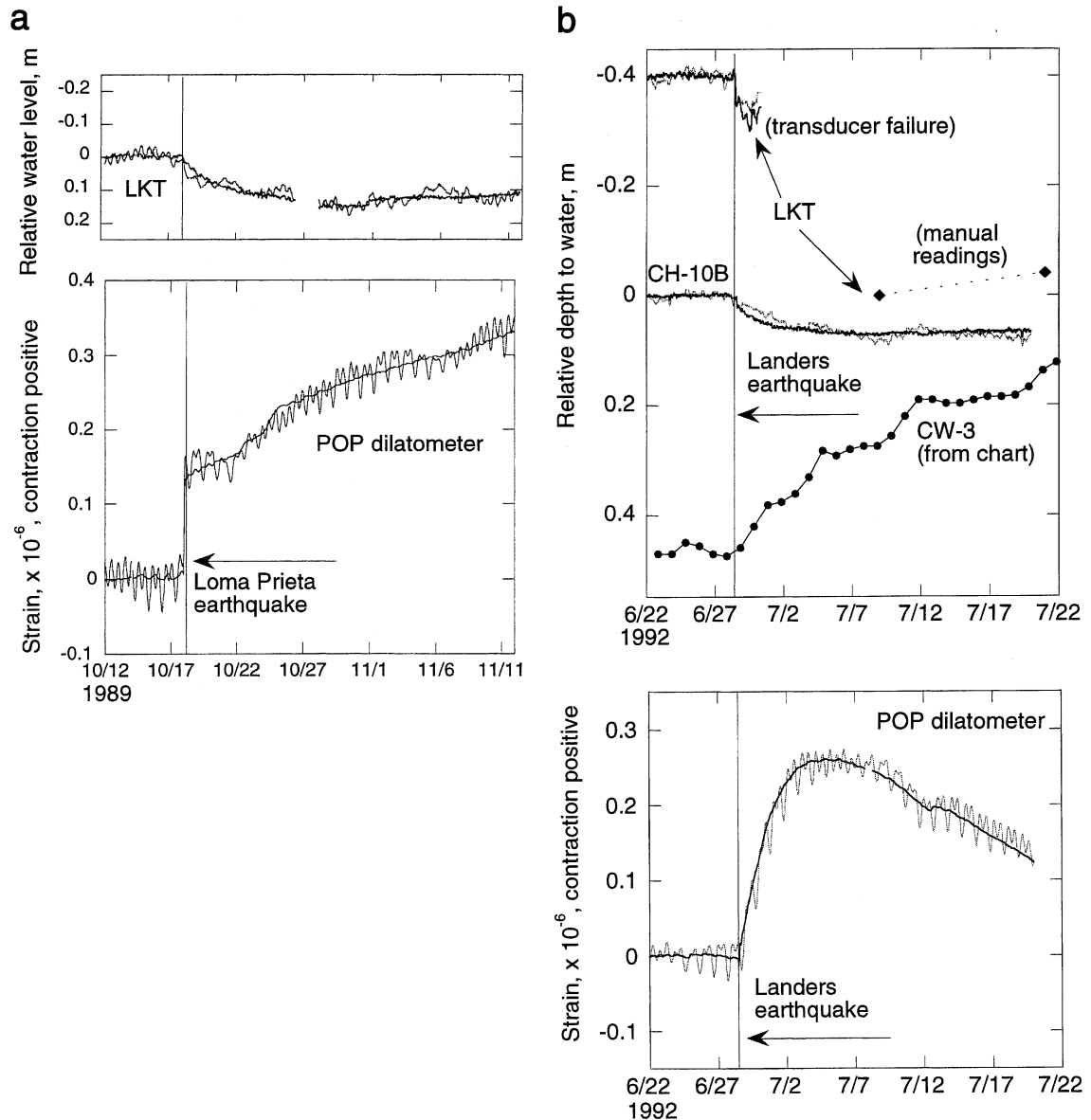


Fig. 7. Graphs showing earthquake-induced water-level and strain changes. Unless otherwise noted, a linear trend has been subtracted from the data to minimize the water-level variation in the 20 days before each earthquake. Data before (gray) and after (black) removal of tidal and atmospheric pressure responses are shown. (a) Loma Prieta earthquake. (b) Landers earthquake. (c) Earthquakes in Long Valley caldera, November–December 1997. (d) M5.6 earthquake of May 15, 1999, southeast of Long Valley. (e) 1999 Hector Mine earthquake. (f) Seismic oscillations in the LVEW following the 1999 Hector Mine earthquake (R. Jacobson, written communication, 1999).

No coseismic steps have been observed at CH-10B, presumably because it is relatively insensitive to strain. For local earthquakes, the directions of coseismic steps are usually consistent with calcu-

lated strain fields for the causative earthquakes. Coseismic strain steps, however, have been recorded by POP for several distant earthquakes. These steps may be artifacts produced by instru-

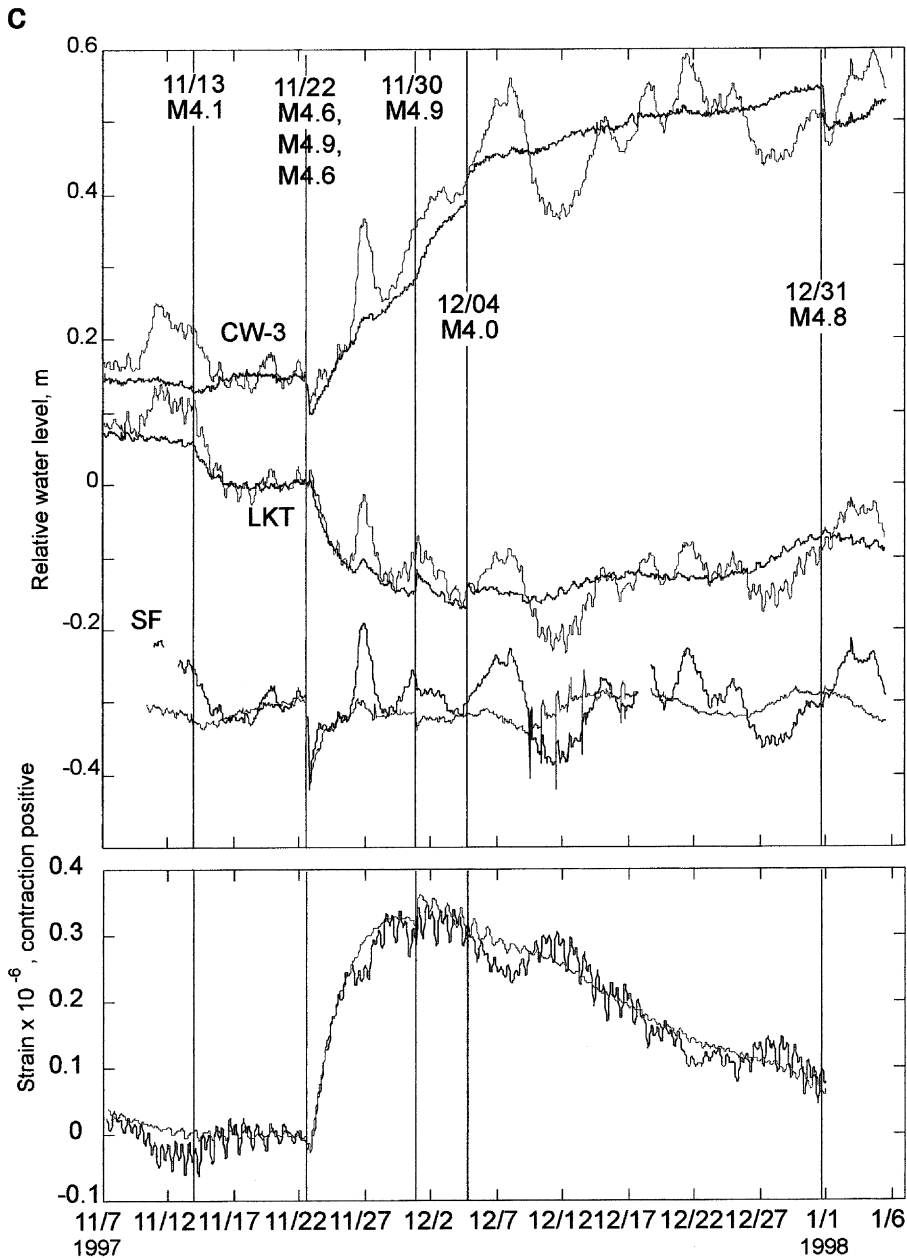


Fig. 7 (Continued).

ment resets induced by large dynamic strains, especially for the instrument at POP prior to September, 1995 (A.T. Linde, personal communication, 2000).

The gradual changes are always down at LKT and CH-10B, and up at CW-3. LKT has the most

consistent response to earthquakes, 10 of which are discernible in the long-term daily data (Fig. 4a). One 6-cm drop resembling a typical post-earthquake change was observed at LKT in late March, 1991, when no earthquake occurred.

Fig. 6a,b shows seismicity at Long Valley for 10

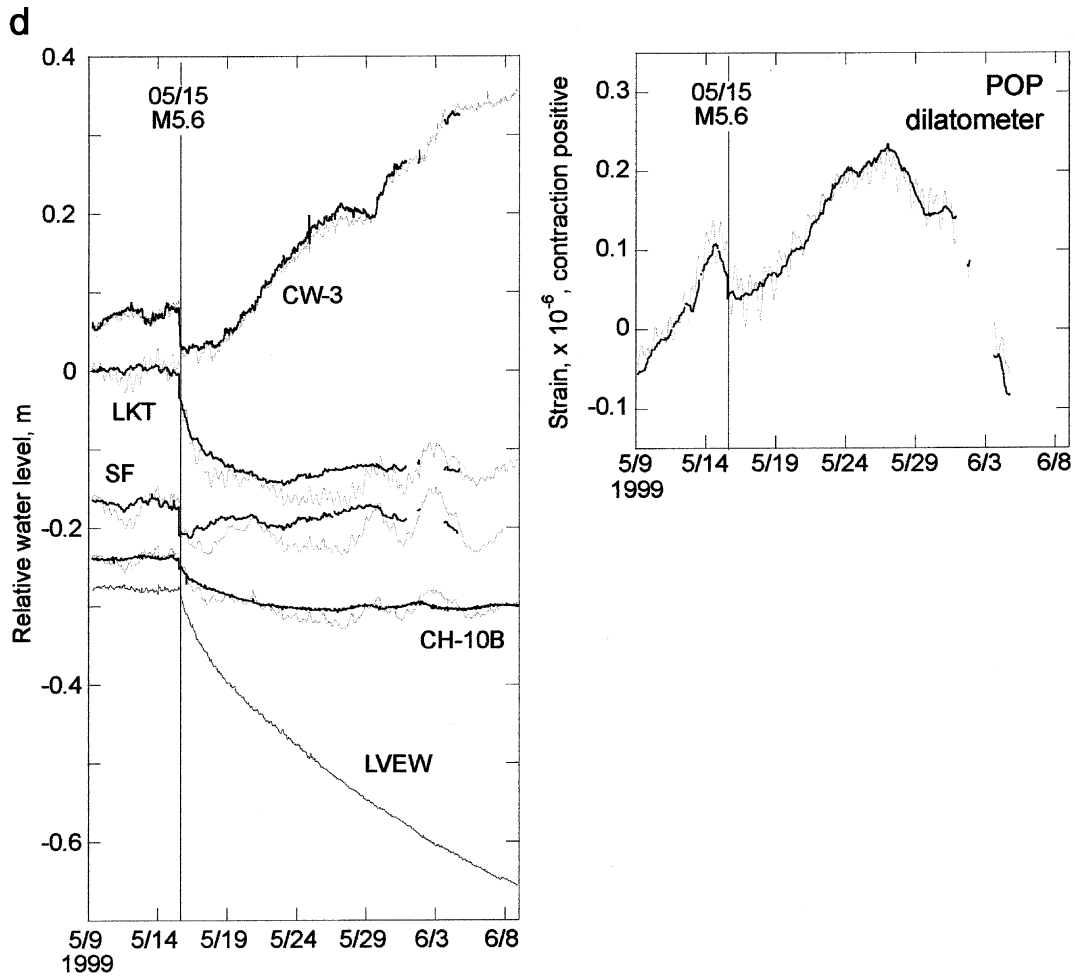


Fig. 7 (Continued).

days following each of the earthquakes listed in Table 1, the time periods when the gradual water-level changes were increasing in amplitude. Seismicity following the distant earthquakes (Fig. 6b) occurs in the same locations as local microseismicity (Fig. 6a). Only for the Landers, Hector Mine, and possibly the Sierra Madre earthquakes did the local seismicity rate increase abruptly following a distant earthquake.

Below we describe a subset of the water-level changes in greater detail.

3.1. 1989 Loma Prieta earthquake

The 1989 M7.1 Loma Prieta earthquake pro-

duced a water-level drop at LKT and a contractional strain-rate change at POP (Fig. 7a). The contractional strain step at POP is likely an instrumental artifact. These data show that the 1992 Landers earthquake was not the first remote earthquake to cause water-level and strain changes at Long Valley.

3.2. 1992 Landers earthquake

The 1992 M7.3 Landers, California, earthquake, triggered a 6-day burst of seismic activity at Long Valley, a strain transient recorded by POP, and water-level changes in the three wells being monitored at that time (Fig. 7b) (Hill et

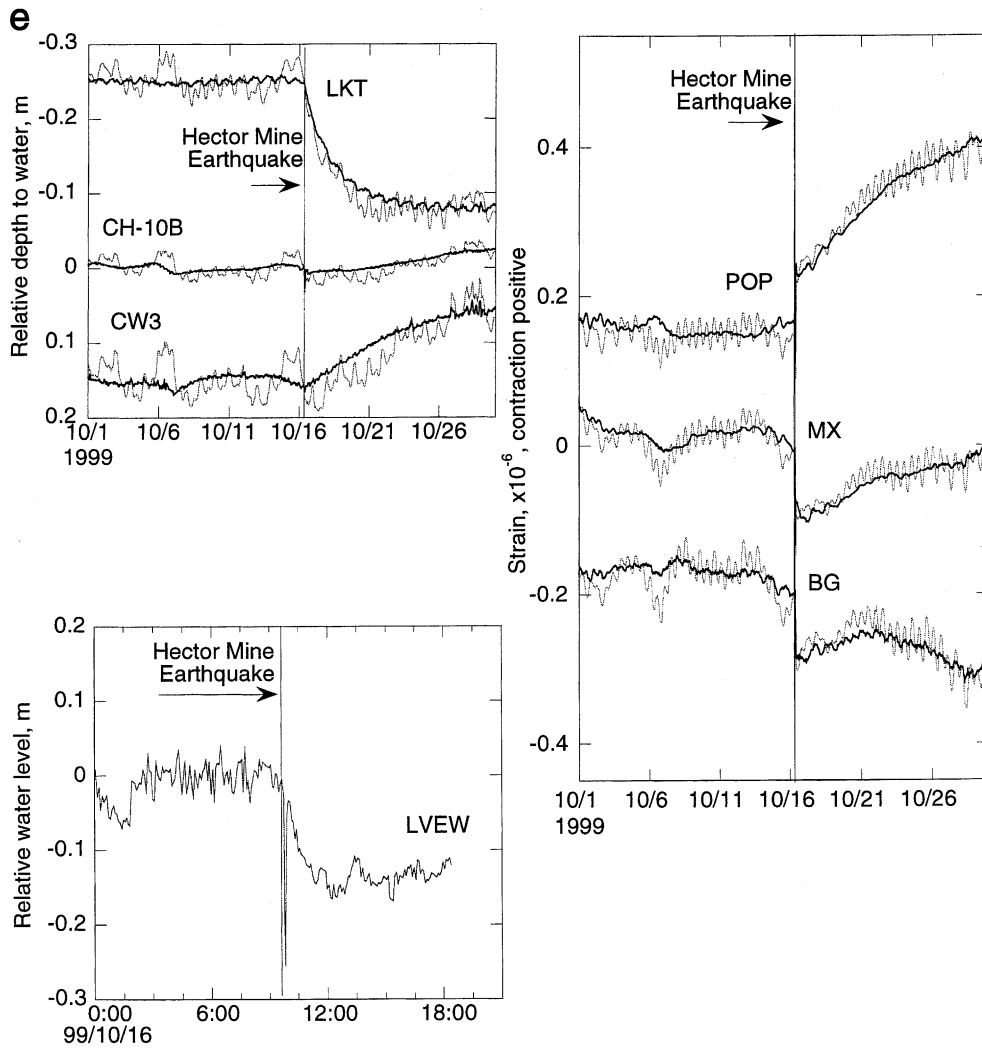


Fig. 7 (Continued).

al., 1995; Roeloffs et al., 1995). The maximum water-level decline at LKT is somewhat uncertain because the transducer failed shortly after the Landers earthquake, but a lower bound based on manual measurements is 0.396 m. This is the largest earthquake-induced water-level change observed at LKT, and, as will be shown in Section 4, is also large relative to the general relationship between the amplitude of water-level change, and the earthquake magnitude and distance. Only a paper chart record is available for CW-3, but digitized values show a gradual

water-level rise beginning after the Landers earthquake.

The largest seismic event triggered by the Landers earthquake in Long Valley was M3.7, smaller than any other local events that have produced water-level drops at LKT. Consequently, we attribute the LKT water-level drop to the seismic waves from the Landers earthquake itself or to aseismic deformation triggered by those waves.

No water-level data from LVEW (then 2375 m deep) are available for the Landers event, but a temperature log on July 19, 1992, revealed a ther-

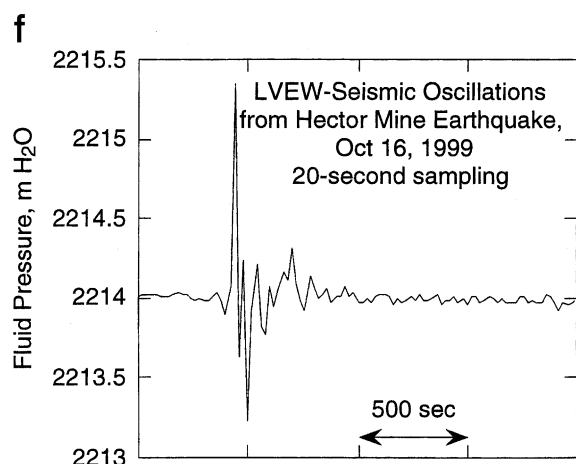


Fig. 7 (Continued).

mal perturbation consistent with increased high-temperature water at depths of 1500–1900 m, compared with an earlier log on January 18, 1992 (Johnston et al., 1995). Casing damage has not been ruled out as a cause of the perturbation.

3.3. Seismic swarm activity in fall 1997

During a vigorous seismic swarm at Long Valley in November 1997 several earthquakes of $M > 4$ occurred in the south moat, but only two were followed by gradual water-level and strain changes. Earthquakes on November 13 and 22 caused both step-like and gradual changes, but a M4.9 on November 30 produced only step-like responses (Fig. 7c). This observation suggests that the process causing the gradual responses requires a recovery period before it can be activated again by seismic waves.

Comparing the water-level and strain data for November 21–25 with the depth of seismicity (Fig. 8) reveals that a M4.6 earthquake on November 22 at 12:06 UT produced coseismic steps at SF and CW-3, but did not initiate gradual water-level or strain changes. Following this earthquake, the seismicity rate increased abruptly, but activity remained concentrated 6–10 km beneath the surface. Five hours later, a M4.9 earthquake at 17:20 UT produced immediate step-like responses followed by gradual water-level

changes. Seismicity rapidly spread upward to within 5 km of the surface, and by the beginning of November 23 had shallowed to 4 km (Prejean, 2002).

Dreger et al. (2000) observed that the seismic events at 12:06 and 17:20 UT on November 22 both had emergent onsets and focal mechanisms with significant isotropic components indicating opening of the fault planes by 5–10 cm. The distinctive feature of the 17:20 event, which produce the largest water-level and strain response, is the subsequent shallowing of seismicity, consistent with upward movement of fluid into or around the seismically active plane.

Accelerated deformation was also recorded on the two-color EDM network (Fig. 9), interpreted as accelerated inflation beneath the resurgent dome between November 22 and 30 (Langbein, 2003 – this issue). The gradual water-level changes that began on November 22, 1997 are the only ones coinciding with detectable deformation on the two-color EDM network. They are also among the largest such changes, so we speculate that they differ primarily in amplitude, rather than mechanism, from the other earthquake-induced changes. If this is correct, the intensified seismic activity and accelerated deformation indicate that upward flow of fluid and accelerated dome deformation may occur with all of the gradual water-level and strain changes.

3.4. M5.6 earthquake on May 15, 1999

This earthquake southeast of the caldera was the first for which water-level data are available from the LVEW. The pattern of gradual water-level changes following this earthquake is similar to other events (Fig. 7d), although at POP only the coseismic step appears significant relative to other variations in the data. At CW-3, water level began to rise 4 days after the earthquake, in contrast to the other earthquake-induced changes, which begin immediately. Comparing Fig. 7d and the long-term hydrograph (Fig. 4a) reveals that water level at CW-3 typically rises in late spring due to recharge from snowmelt. The 4-day delay between the earthquake and the onset of the water-level rise, and the longer duration of

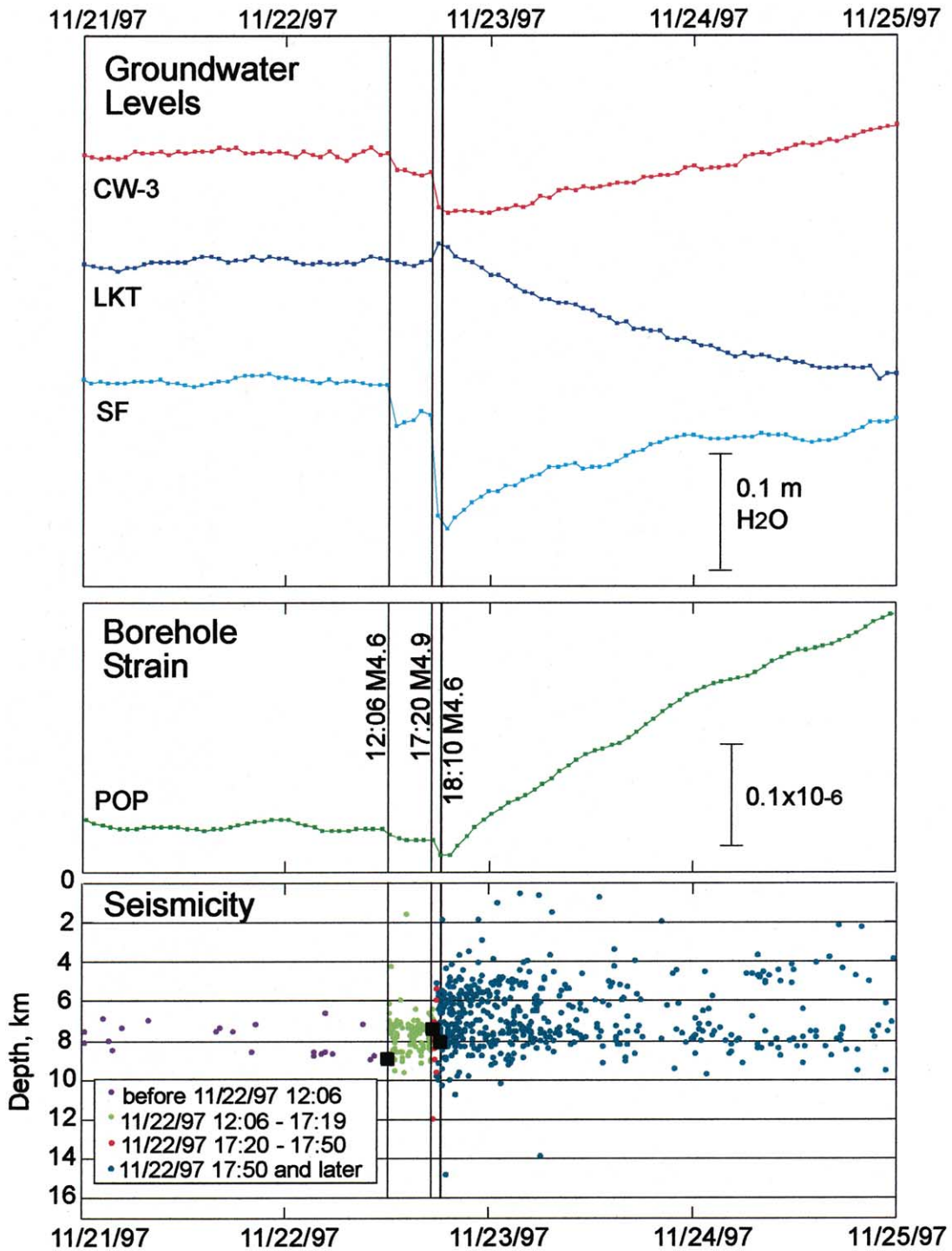


Fig. 8. Water-level and seismicity data for November 21–25, 1997 (relocated hypocenters courtesy of S. Prejean, USGS).

the elevated water level suggest this water-level increase at CW-3 might have been due to recharge, rather than to the earthquake.

The detrended water level in LVEW dropped 5 cm in three days following the earthquake, and then continued to decline. Although fluid level was rising rapidly to re-equilibrate with formation pressure after drilling, and was measured only once every 30 min, the observed change shows that the process causing the earthquake-induced water-level changes is not limited to weathered or unconsolidated near-surface rocks.

3.5. October 16, 1999, Hector Mine earthquake

The 1999 M7.1 Hector Mine, California, earthquake triggered microseismicity at Long Valley (Gomberg et al., 2001), and also caused water-level and strain changes (Fig. 7e). The water-level changes were, as usual, a drop at LKT and a rise at CW-3. No data are available for SF. By coincidence, a high-resolution quartz pressure transducer was being tested in the LVEW during the Hector Mine earthquake (R. Jacobson, written communication, 1999), and recorded a seismic oscillation, followed by a 0.13-m water-level drop that stabilized a few hours after the earthquake. All three strainmeters operating then recorded abrupt steps at the time of the earthquake, with contraction at POP, outside the caldera, and extension at MX and BG, near the caldera rim. The MX and BG strainmeters have a two-stage design that can record step-like changes without interference from dynamic strain. A contractional strain-rate change followed the step at POP and may have occurred at MX as well.

4. Consistent features of the gradual water-level changes

The water-level changes in Long Valley induced by distant earthquakes, including the Landers earthquake, strongly resemble those accompanying local seismicity. In this section, we show that the gradual water-level changes have repeatable time histories from event to event, and that the

water-level changes generally increase with earthquake magnitude and proximity.

4.1. Time histories of the gradual changes

Roeloffs (1998) showed that at the BV well near Parkfield, California, the time history of earthquake-induced water-level rises is very similar from one earthquake to another. Fig. 10a–d shows the best-recorded earthquake responses for LKT, CW-3, CH-10B, and POP, respectively. The responses have been superimposed after subtracting linear trends fit to about 20 days of data preceding each earthquake, and dividing by the maximum water-level or strain excursion. Data from LVEW exist for only the M5.6 earthquake on May 15, 1999, and the Hector Mine earthquake. The more rapid response to the Hector Mine event is probably caused by different instrumentation and borehole conditions.

The time histories of all seven of the gradual earthquake-induced water-level responses at LKT are essentially identical for at least the first 40 days after each earthquake. The water level reaches a minimum after 8–12 days, and then recovers about 70% of the drop over the next 70 days. The apparent slow recovery of the response to the Landers earthquake could result from incorrect scaling. After about 55 days, the response to the earthquake on November 22, 1997, at 17:20 appears to recover more quickly than the others, but continuing seismic activity at this time might have influenced the recovery rate.

The water-level rises at CW-3 following the 1992 Landers earthquake, the earthquake on February 10, 1997, and the 1999 Hector Mine earthquake have nearly identical shapes for the first 40 days after each event. The response to the M4.9 event on November 22, 1997, also has a similar time history for the first 30 days after the earthquake. Following the M5.6 earthquake on May 15, 1999, the water level did not begin to rise until May 19, and recovered relatively slowly, suggesting this response may actually be a seasonal recharge event unrelated to the earthquake. Except for the 1994 Northridge earthquake, which produced the fastest water-level rise, the gradual

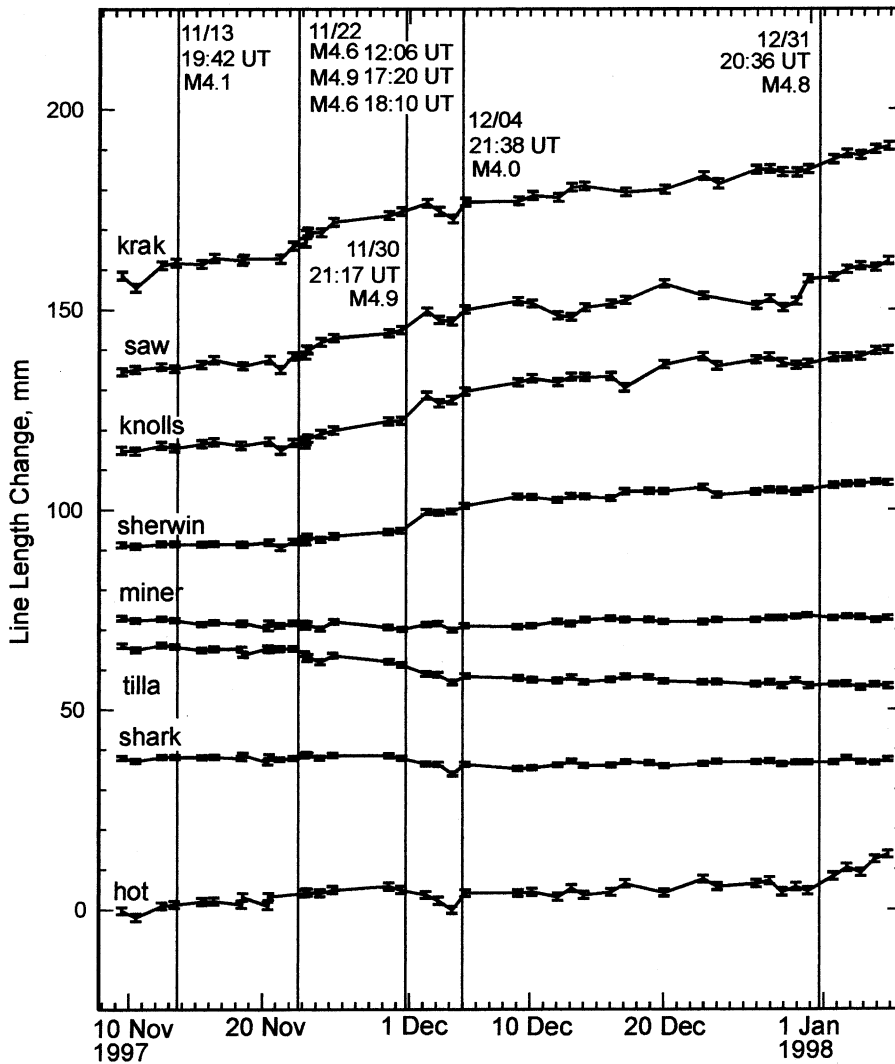


Fig. 9. Two-color EDM measurements for November 8, 1997, to January 7, 1998 (data courtesy of J. Langbein, USGS).

changes at CW-3 take 20–30 days to reach maximum values.

At CH-10B only the 1992 Landers earthquake and the M5.6 event on May 15, 1999, produced significant responses, which are nearly identical for the first 25 days and reach minimum values after 9–11 days. After 25 days, the hydrographs for the two earthquakes diverge with abrupt slope changes. These abrupt changes are not uncommon in the CH-10B hydrograph and seem unrelated to earthquakes.

The strain responses at POP are of two types.

One type is the transient change observed following the 1992 Landers earthquake and the M4.9 earthquake on November 22, 1997, at 17:20 UT (Fig. 10d). The contractional portions of these two curves have nearly identical time histories, and the recovery rates are also similar, if the additional coseismic step for the earthquake on November 30, 1997, is allowed for. Both transients peak 5–7 days after the respective earthquakes, a shorter time constant than water levels in LKT, CH-10B, or CW-3. The other type of response is a step complete within an hour after each earth-

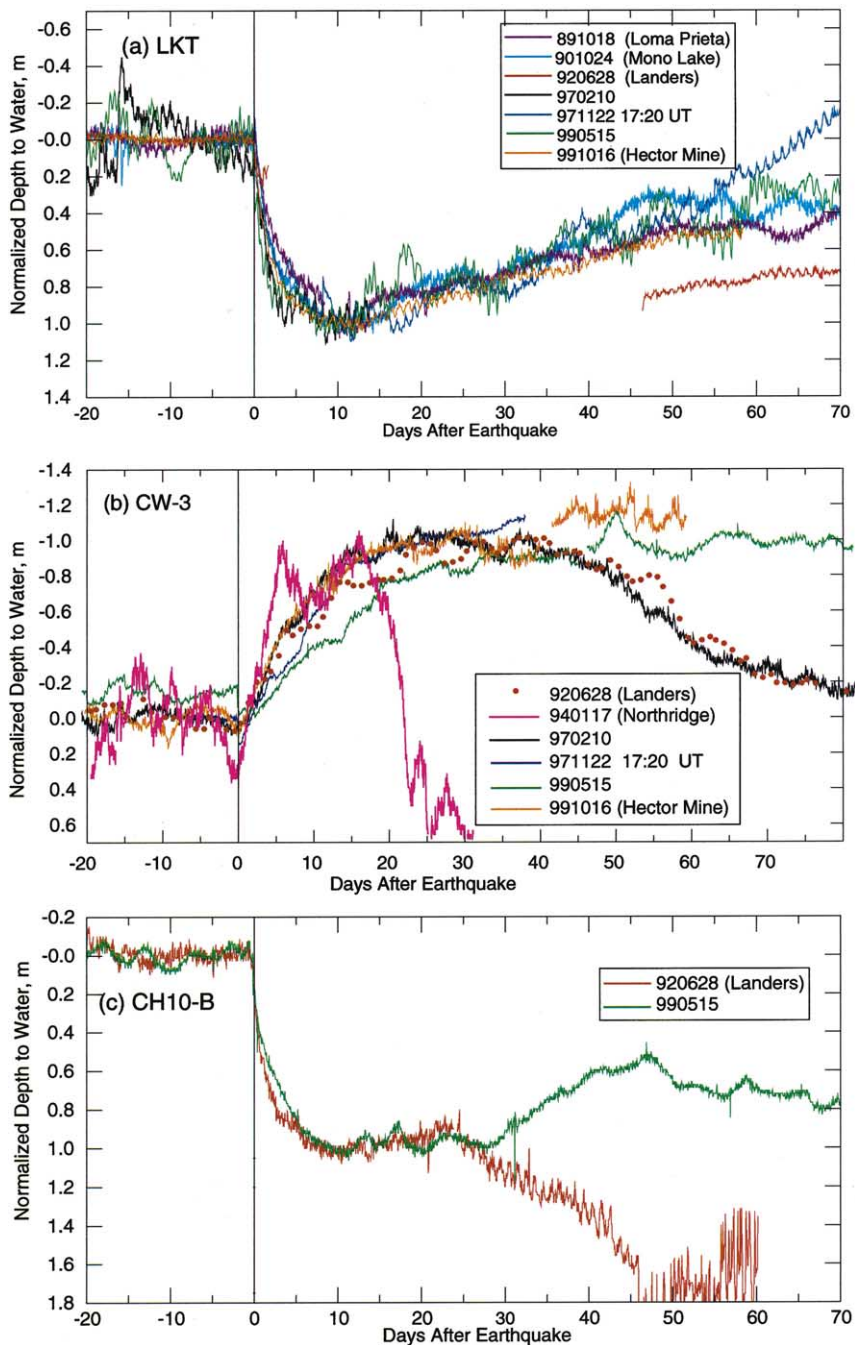


Fig. 10. Superpositions of normalized water-level and strain changes. All curves have had a linear trend removed from the 20 days preceding each earthquake. Each curve has been divided by the absolute value of its maximum excursion, except as noted. (a) LKT water level. (b) CW-3 water level. Northridge response is scaled by maximum positive value; response to the M4.9 event on November 22, 1997, is scaled to reach unity 25 days after the earthquake. The water-level curve is not shown after 30 days from the earthquake because it was affected by subsequent seismic events. (c) CH-10B. Landers response is scaled by value reached 10 days after the earthquake. (d) POP strain.

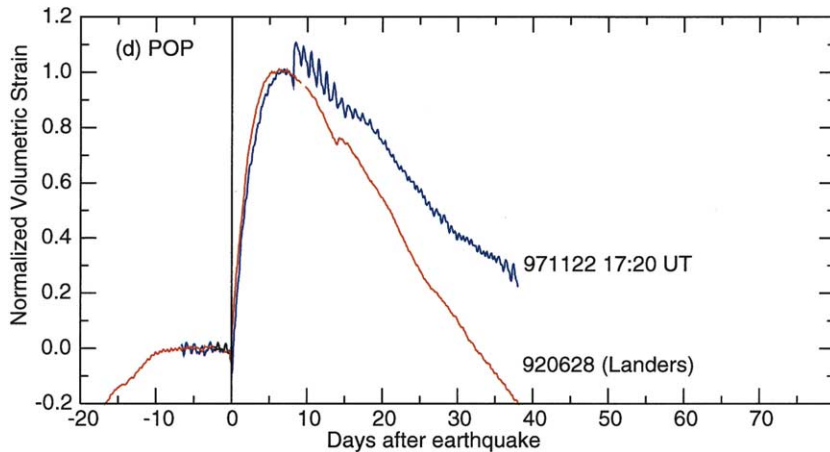


Fig. 10 (Continued).

quake, followed by a contractional strain-rate change. This type of response does not lend itself to superposition and the steps are of questionable significance, but all of the contractional rate changes are smaller than the rate changes represented by the contractional portions of the 1992 Landers and the November 22, 1997, transient responses.

4.2. Dependence on earthquake magnitude and distance

For the BV well near Parkfield, California, the sizes of gradual post-seismic water-level rises are well predicted by a function of earthquake magnitude and distance, and the coefficients in this relationship are consistent with the water-level re-

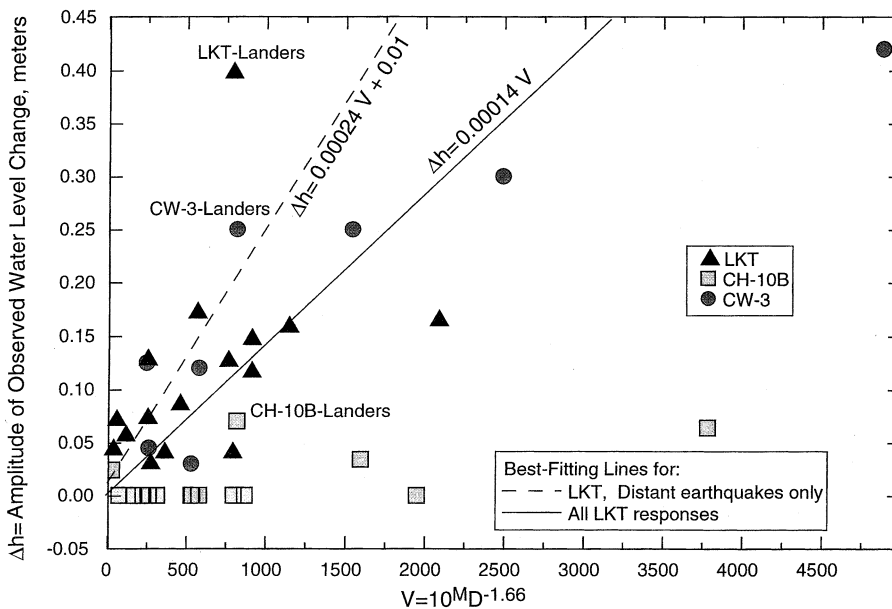


Fig. 11. Dependence of gradual water-level changes on earthquake magnitude and hypocentral distance.

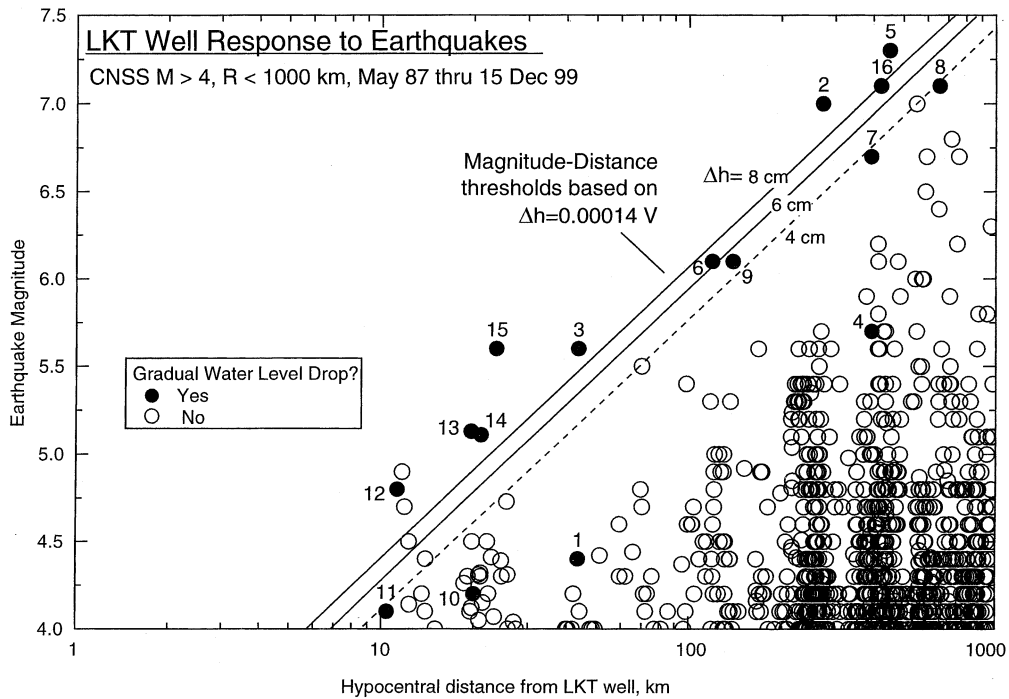


Fig. 12. All earthquakes $M \geq 4$ from the CNSS catalog from May 1, 1987, through December 1, 1999, within 1000 km of LKT, and thresholds for expected gradual water-level drops at LKT based on the best-fitting linear relationship to V . Earthquakes that produced gradual water-level responses are labeled with event numbers from Table 3.

sponse being proportional to peak seismic ground velocity (Roeloffs, 1998). More specifically, earthquake magnitude, M , is computed using:

$$M = \log_{10} A + C_1 \log_{10} D + C_2 \quad (5)$$

where A is the seismic trace amplitude (proportional to ground velocity), D is hypocentral distance in km, and the C_i are constants, with $C_1 = 1.66$ for surface wave magnitude (Bullen and Bolt, 1985). Eq. 5 implies that peak seismic ground velocity is proportional to $V = 10^M D^{C_1}$.

Fig. 11 shows the amplitudes of the water-level changes at Long Valley plotted against V , together with the best-fitting relations for all responses at LKT, and for responses of LKT to distant earthquakes only. LKT and CW-3 have similar dependence on V . CH-10B has a much smaller coefficient; all of the changes at CH10-B are relatively small, and there are many earthquakes with no detectable water-level response, possibly due to the relative insensitivity of CH10-B to

strain. For all three wells, the responses to the Landers earthquake are relatively large when plotted against V , possibly because its strong northward directivity (Gomberg et al., 2001) is neglected in the value of V computed from its magnitude.

In Fig. 12, all earthquakes of $M \geq 4$ in the Council of the National Seismic System (CNSS) catalog within 1000 km of LKT from May 1987 through December 15, 1999, are plotted. Also shown are the expected thresholds for 4, 6 and 8-cm water-level drops based on the best-fitting linear relation expressing all water-level drops at LKT as a function of V . The M4.6 earthquake on November 22, 1997, at 18:10 UT and M4.9 event on November 30, 1997, at 21:17 UT are the only earthquakes expected to cause changes of 8 cm or more that were not followed by gradual water-level drops. Conversely, water-level drops larger than expected occurred for local earthquakes on July 11, 1989, and February 10, 1997, and the 1991 Sierra Madre earthquake.

5. Mechanism of the water-level changes

The occurrence of the gradual water-level changes in five wells, the accompanying strain detected by borehole strainmeters, the coincidence of the largest water-level change with the Landers earthquake, which also triggered six days of enhanced microseismicity, and the accelerated deformation detected by the two-color EDM network in November–December 1997 all suggest that the gradual water-level changes reflect deformation triggered by seismic waves. There are two end-member possibilities for the time scale of such deformation: the deformation might continue for a number of days following the earthquake; alternatively, the fluid-pressure changes might represent re-equilibration of a pressure field set up by strain that occurs primarily during the passage of seismic waves.

The borehole strain data show that during the seconds to minutes that seismic waves from distant earthquakes shake Long Valley, they can produce strain-rate changes that outlast the seismic shaking by many orders of magnitude. However, strain-rate changes or transient strain changes could be caused by fluid-flow effects. On the other hand, the recorded strain steps, if real, would strongly indicate step-like strain of the rock matrix. Strainmeter, water-level, and GPS data from the Izu peninsula in Japan during seismic swarms have time histories resembling the water-level changes at Long Valley, and can be explained by upward propagation of dikes, without appealing to pressure-deformation coupling (Okada and Yamamoto, 1991; Aoki et al., 1999; Koizumi et al., 1999).

The step-like coseismic water-level changes due to local earthquakes show that LKT, CW-3, and SF can track step-like changes in strain. However, the time histories of the water-level changes caused by distant earthquakes are not step-like. Earthquakes could induce step-like strain changes of no more than 0.04×10^{-6} without causing an (observable) 0.02-m water-level change at LKT. The total excursions of several of the water-level changes at LKT are as large as 0.1–0.17 m. If the strain sensitivity of LKT is typical of nearby parts of the caldera, then extensional strain of 0.2–0.35

$\times 10^{-6}$ could produce undrained fluid-pressure changes this large, which could gradually diffuse to LKT.

To infer the mechanism of the water-level changes, we begin in Section 5.1 by showing that the time history of water-level changes in LKT can be matched by diffusion of pressure drops that occur ‘instantaneously’ after earthquakes. In Sections 5.2 and 5.3 we show that the water-level changes caused by distant earthquakes can largely be accounted for by two processes: diffusive re-equilibration of a pressure drop caused by accelerated inflation of the resurgent dome, and a localized pressure increase in the south moat, likely attributable to thermal pressurization. In Section 5.4, we consider the possible role of south moat faulting in producing the water-level changes.

5.1. Diffusive response at LKT to step-like coseismic changes

To constrain the size and location of undrained fluid-pressure changes that could lead to the observed gradual water-level drops at LKT, we used a solution given by Roeloffs (1998) to compute the expected time history for decay of a localized pressure drop occurring instantaneously in a 1D aquifer with no-flow and discharge boundaries separated by a distance L (Fig. 13a). The overall time scale of the fluid-pressure change is proportional to L^2/c . In the model, the water-level change recovers to zero by diffusion of the pressure disturbance throughout the hydrologic system. For fixed c , the time scales of the fluid-pressure drop and recovery depend on the distances from the pressure pulse to the well and to the boundaries of the flow system, respectively. The repeatable shape of the water-level curves implies that the hydrologic disturbance caused by the seismic waves occurs in the same location for each earthquake.

The fit to the LKT water-level response (Fig. 13b) was obtained with $L^2/c = 10^7$ s, or 113 days, $x_w = 0.64L$, and the coseismic pressure disturbance extending from $x = 0$ to $x = 0.5L$. The model is very sensitive to the distance from the well to the near edge of the disturbance. The best-fit pa-

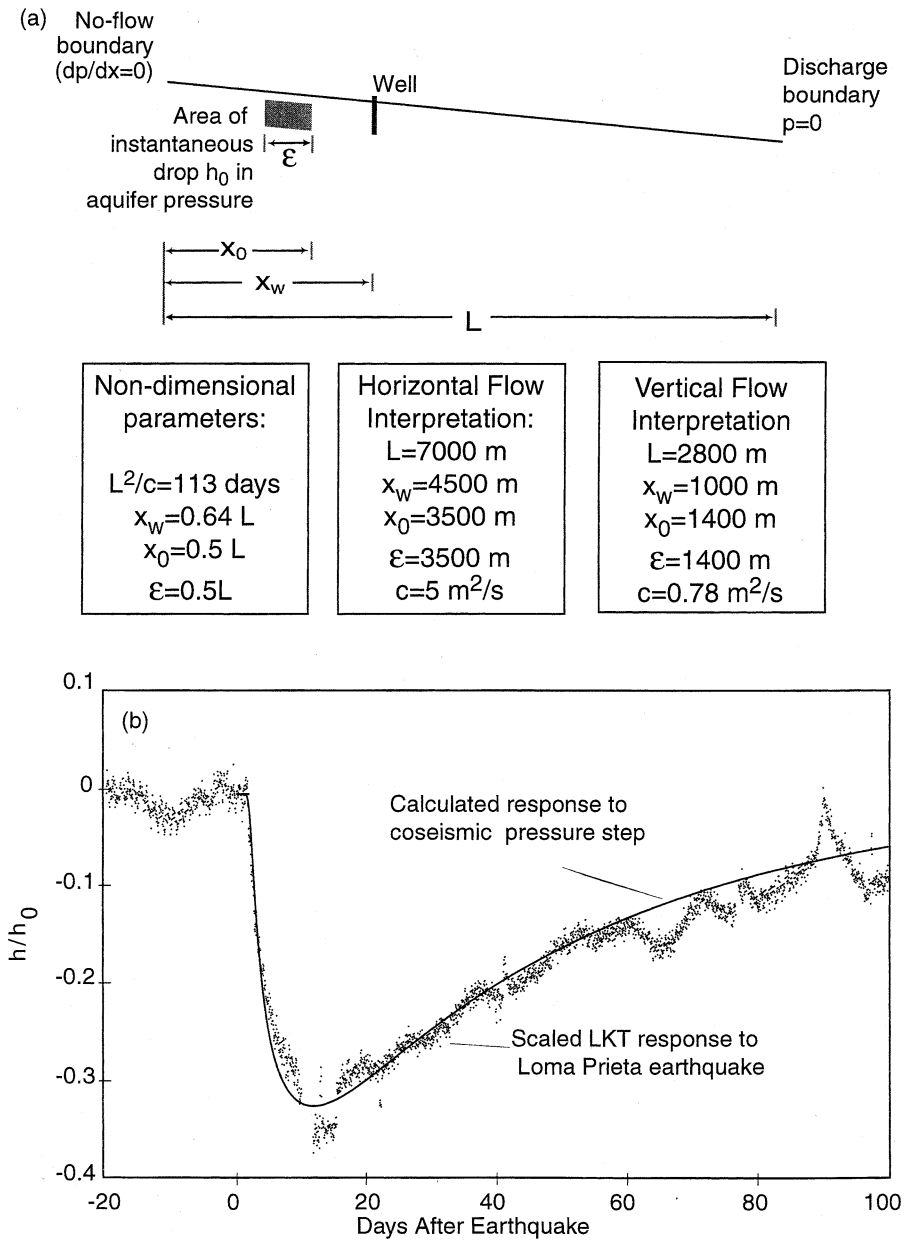


Fig. 13. (a) Diagram showing boundary and initial conditions for a one-dimensional pressure-pulse decay model. (b) Fit of the model to the response of the LKT well to the Loma Prieta earthquake.

parameters could be interpreted as representing a horizontal flow system in which fluid enters the groundwater system on the resurgent dome, flows northwest, and discharges into the Owens River about 7 km away. The value of $x_w=0.64 L$ is consistent with the well's location 2.5 km from

the river, and the horizontal hydraulic diffusivity required to match the time scale is $5 \text{ m}^2 \text{ s}^{-1}$, which is consistent with the diffusivities inferred for LKT (Section 2.4). The coseismic pressure drop would extend from the center of the resurgent dome to within 1 km of LKT, approximately

the location of extensional strain accompanying dome inflation. Alternatively, the model could represent a vertical flow regime. If the LKT water level represents fluid pressure at a depth of 1000 m, then L would be 2.8 km, the vertical diffusivity would be $0.78 \text{ m}^2 \text{ s}^{-1}$ and the fluid-pressure change would have its upper edge 1.4 km below the surface. In the vertical interpretation, the responses at LKT represent diffusion of earthquake-induced changes that occur more rapidly at depth, and the similar time histories at LKT and CH-10B could be accounted for by

a source under the dome at an approximately uniform depth, although this leaves the slower water-level rises at CW-3 unaccounted for.

Regardless of the physical interpretation, Fig. 13b shows that the pressure change at LKT is only 0.3 times the amplitude of the coseismic pressure drop. Even using the large strain sensitivity for LVEW, $2 \text{ m}/10^{-6}$, the extensional volumetric strain required to lower water level 0.3–0.54 m would be $0.15\text{--}0.27 \times 10^{-6}$. The two-color EDM detection threshold is about 1-mm linear extension of the 7.8-km CASA-KRAK line, corre-

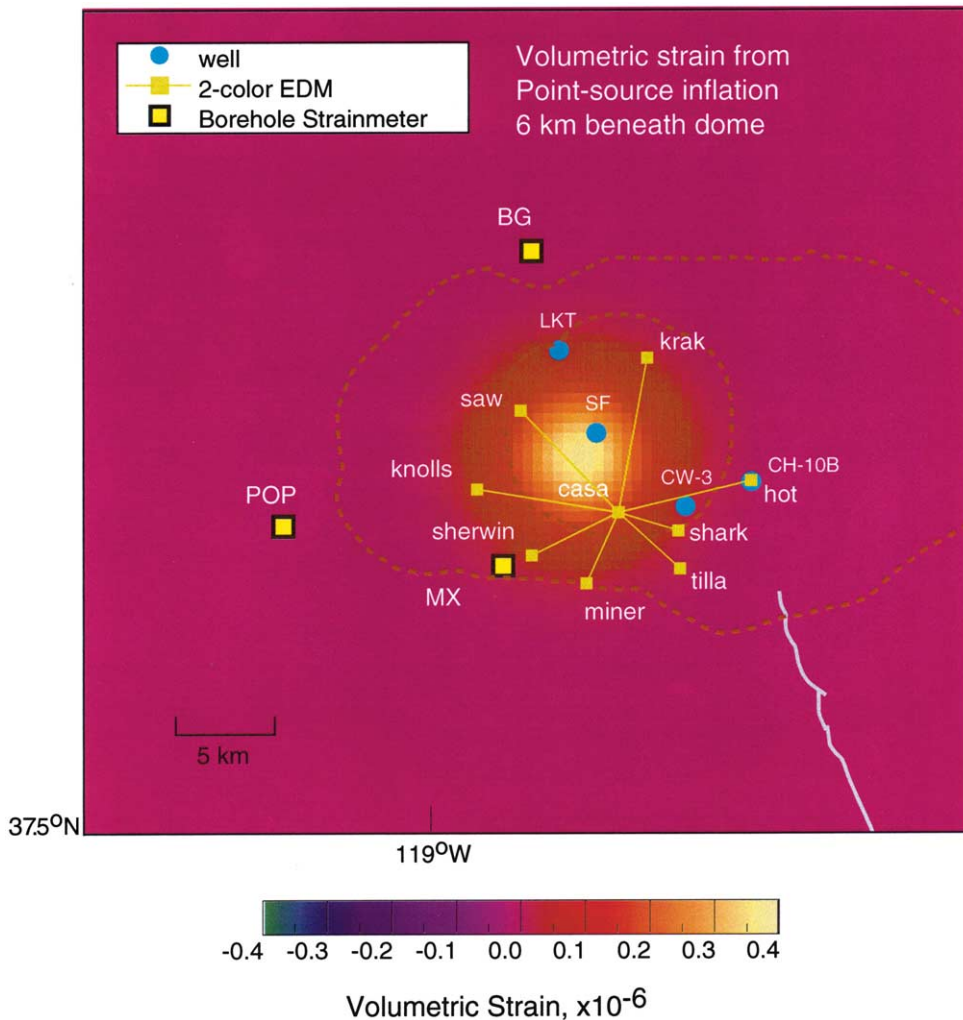


Fig. 14. Map of the volumetric strain field imposed by inflation of a point source centered at 6 km depth below the resurgent dome, with strength sufficient to lengthen the two-color EDM line to SAW by 1 mm.

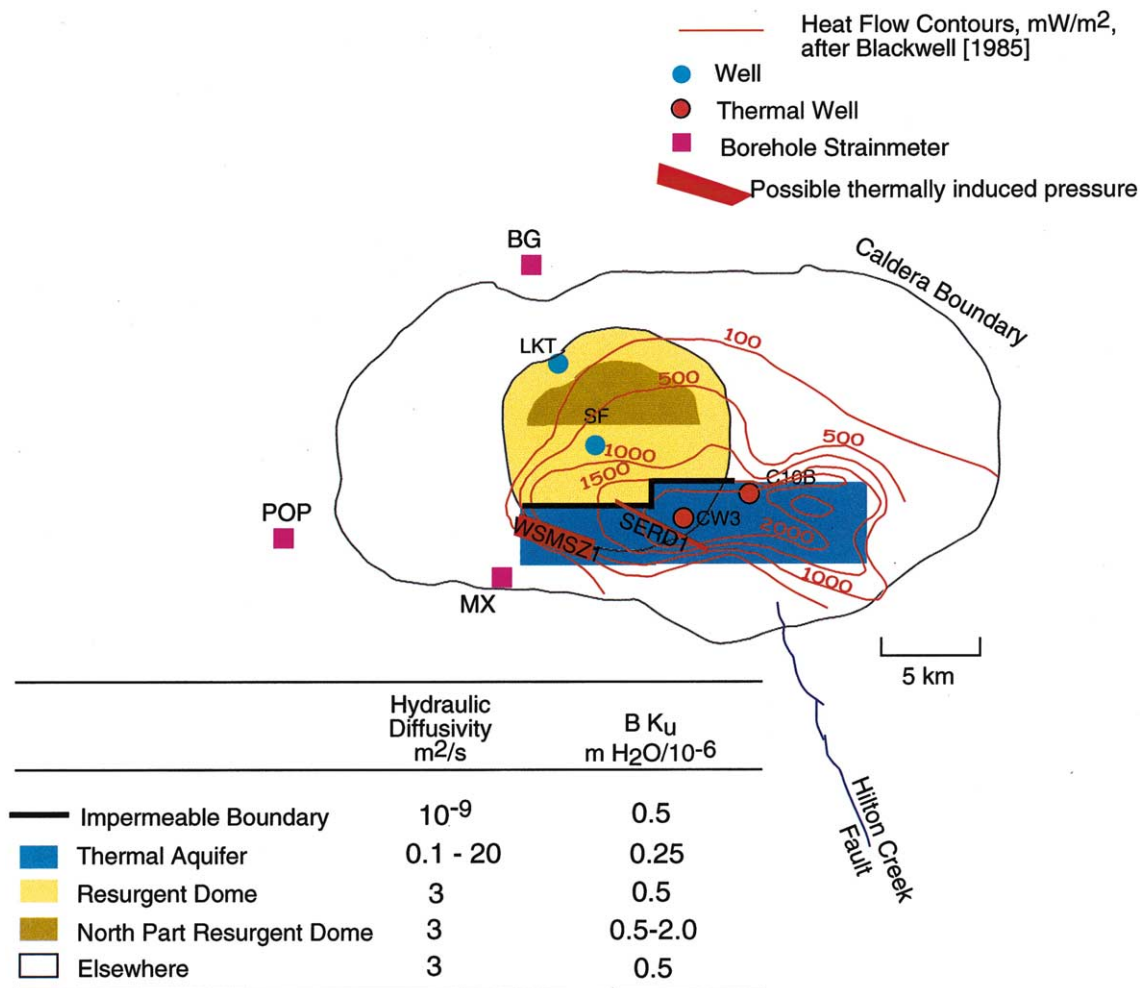


Fig. 15. Features included in the 2D finite element model used to compute fluid diffusion.

sponding to 0.13×10^{-6} linear strain. Thus, diffusion of undrained pore pressure due to dome deformation below the two-color EDM detection threshold can just produce a water-level drop of 0.1 m at LKT, and cannot account for the 0.4-m drop induced by the Landers earthquake. This conclusion is independent of the source deforming the dome.

The good fit to the LKT data obtained with the 1D model demonstrates that the water-level changes can be entirely explained by the diffusion of a nearby instantaneous pressure change. On the other hand, it is also obviously possible to account for the water-level changes as proportion-

al to a strain field having the same time history, with no accompanying diffusion. Without independent knowledge of the hydraulic diffusivity, these two alternatives cannot be distinguished.

The possibility also exists that seismic waves change permeabilities, but Roeloffs (1998) showed that the expected response to an instantaneous change of permeability is more gradual than the diffusive response to a strain step. Permeability changes would influence the earth tide responses of the wells, but analysis to date has not revealed changes in the tidal responses accompanying earthquakes. It is likely that local earthquakes change permeability in the vicinity of their hypo-

centers, but such changes are too distant from the observation wells to account for the observed gradual post-earthquake changes.

5.2. Water-level drops at LKT: diffusive response to dome extension

Motivated by the evidence for accelerated dome inflation and upward movement of fluid at the time of the November 22, 1997, water-level and strain changes, we show in this section that the water-level drops at LKT can largely be accounted for by diffusion of pressure drops on the dome during episodes of incremental inflation.

Although between November 22 and 25, 1997, 4–5 mm of lengthening occurred on the two-color EDM lines to SAW and KRAK, no observable (> 1 mm) line-length changes accompanied any of the other earthquake-induced water-level changes. The exact depth and geometry of inflation sources beneath the dome depends on the geodetic data subset used, so for simplicity we assume a point inflation source at a depth of 6 km. Fig. 14 shows the strain field of this source with a strength that lengthens the line to SAW by 1 mm, computed using a code written by Okada (1992).

Assuming the incremental inflation occurs instantaneously, we multiply the resulting volumetric strain field by a strain sensitivity (Eq. 1) to obtain an undrained fluid-pressure field throughout the Long Valley area. Using a 2D finite element model with this fluid pressure as an initial condition, we calculate the time-dependent pressure changes accompanying its diffusive re-equilibration to pre-earthquake conditions by horizontal flow.

Two material properties were adjusted in the model (Fig. 15). The amplitude of the initial fluid pressure is governed by BK_u , and the time scale of pressure dissipation is governed by the (horizontal) hydraulic diffusivity, c . We allow the thermal aquifer to have distinct properties, as discussed below. In the model, the boundary of the thermal aquifer was chosen based on the location of heat-flow contours (Blackwell, 1985).

The simplest simulation (Fig. 16a) has $BK_u = 0.5 \text{ m}/10^{-6}$ everywhere except in the ther-

mal aquifer, where it is assigned a value of $0.25 \text{ m}/10^{-6}$, the strain sensitivity of CW-3. The hydraulic diffusivity was adjusted to $3 \text{ m}^2 \text{ s}^{-1}$ to match the time dependence of the fluid-pressure change at LKT. This model accurately simulates the time dependence of the changes at LKT except that it begins with a step. Since no step is generally observed, the inflation may actually occur more gradually. The simulation also underestimates the amplitude of the change at LKT. No fluid-pressure rise is simulated at CW-3.

A second simulation (Fig. 16b) assigns the north half of the dome a higher value of $BK_u = 2.0 \text{ m}/10^{-6}$, slightly below the strain sensitivity at LVEW. The resulting larger initial pressure drop on the dome leads to a larger fluid-pressure decrease at LKT of 0.07 m. This still underestimates the observed changes at LKT, several of which are 0.15 m or more in amplitude. However, there are no obvious changes to the model that could produce a larger rise without also producing more displacement of the two-color lines. The discrepancy could be resolved with a more complex model having such features as anisotropic permeability providing a more direct flow path to LKT, but in view of the limited data we chose not to pursue this further.

Both simulations in Fig. 16 underestimate the time for water level to recover at SF, probably because at SF the vertical flow, which is not being simulated, dominates the rate of recovery.

5.3. Water-level rises at CW-3: evidence for thermal pressurization

Dome inflation cannot account for the water-level rises at CW-3. More generally, if the water-level rises at CW-3 indicate contractional volumetric strain, then this would be the only site inside the caldera where contraction is observed repeatedly. The gradual post-earthquake changes at all other wells are water-level drops, consistent with crustal extension, and the two new dilatometers at the caldera boundary also exhibited extension during the Hector Mine earthquake. The sources that dominate the two-color EDM data – inflation under the dome, and right-lateral slip in the south moat – impose extensional volumetric

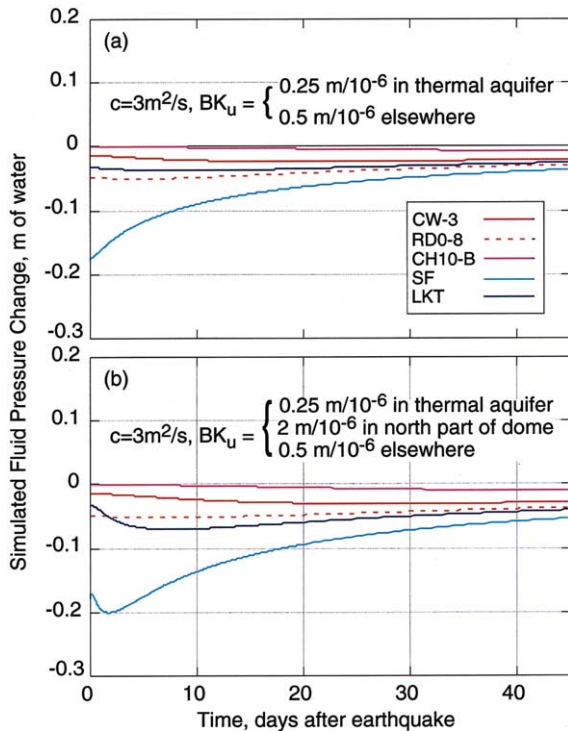


Fig. 16. Simulated time histories of fluid pressure at observation wells with undrained pore pressure field from dome inflation as initial condition. (a) Simulation with uniform diffusivity. (b) Simulation with higher BK_u on the northern part of the resurgent dome.

strain at CW-3. Moreover, CW-3 is located on the two-color EDM line from CASA to HOT, which lengthened during the 1997–1998 episode.

We show in this section that the post-earthquake water-level rises at CW-3 can be accounted for by diffusion of elevated pressure induced by earthquakes at discrete locations in the south moat hydrothermal system. Contractional strain that could produce this elevated pressure is contraindicated by several lines of evidence, so another process is required. We propose that the fluid-pressure increases originate with thermal pressurization of pore fluid due to upward movement of magma or hot aqueous fluid into subvertical structures in the south moat.

Delaney (1982) evaluates the pressure fields due to thermal expansion of pore fluid adjacent to a planar intrusion. Because the pressurized fluid can flow away from the intrusion, the fluid-tempera-

ture increase and thermally induced pressure are limited. The hot intrusion thus behaves as a plane of fixed pressure until the onset of fluid convection.

The effect of thermal pressurization can therefore be modeled by including nodes at which the pressure is constrained to ramp up to a maximum value over a 12-h period and then remain fixed. It is also essential to place a barrier to flow between the thermal aquifer and wells LKT, SF, and LVEW. Impediments to such flow are consistent with the lower temperatures in these wells, but the data considered here provide no further constraints on the configuration or location of such a barrier. The assumed barrier (Fig. 15) is 500 m wide and at that width must have a diffusivity of $10^{-9} \text{ m}^2 \text{ s}^{-1}$ to prevent the increased fluid pressure in the south moat from influencing the water level at LKT and SF.

We first consider a fluid-pressure source above plane WSMSZ1 (Fig. 15), where seismicity abruptly spread to shallower depths coincident with the onset of water-level changes on November 22, 1997. The time history and amplitude of the water-level change at CW-3 can be fit by adjusting the amplitude of the pressure source to 0.76 m of water and the diffusivity of the thermal aquifer to $20 \text{ m}^2 \text{ s}^{-1}$ (Fig. 17a). However, this model predicts an unobserved pressure increase at CH-10B. To reduce this pressure increase, we impose a zero pressure boundary (Fig. 15) to simulate the thermal spring discharge area near Hot Creek gorge. The simulated fluid pressures are shown in Fig. 17b. The model would predict increased discharge at the eastern end of the thermal aquifer; data from 1992 do show that stage in the Hot Bubbling Pool rose following the Landers earthquake (Roeloffs et al., 1995).

The simulated water-level rise at CW-3 generally matches the observations, but an important detail is a calculated delay of about 1 day due to the distance over which the pressure increase diffuses. The simulated curve does resemble that recorded following the M5.6 earthquake on May 15, 1999, but water-level rises after other earthquakes begin much more abruptly.

Data from well RDO-8, an intermittently monitored well completed in the geothermal aquifer,

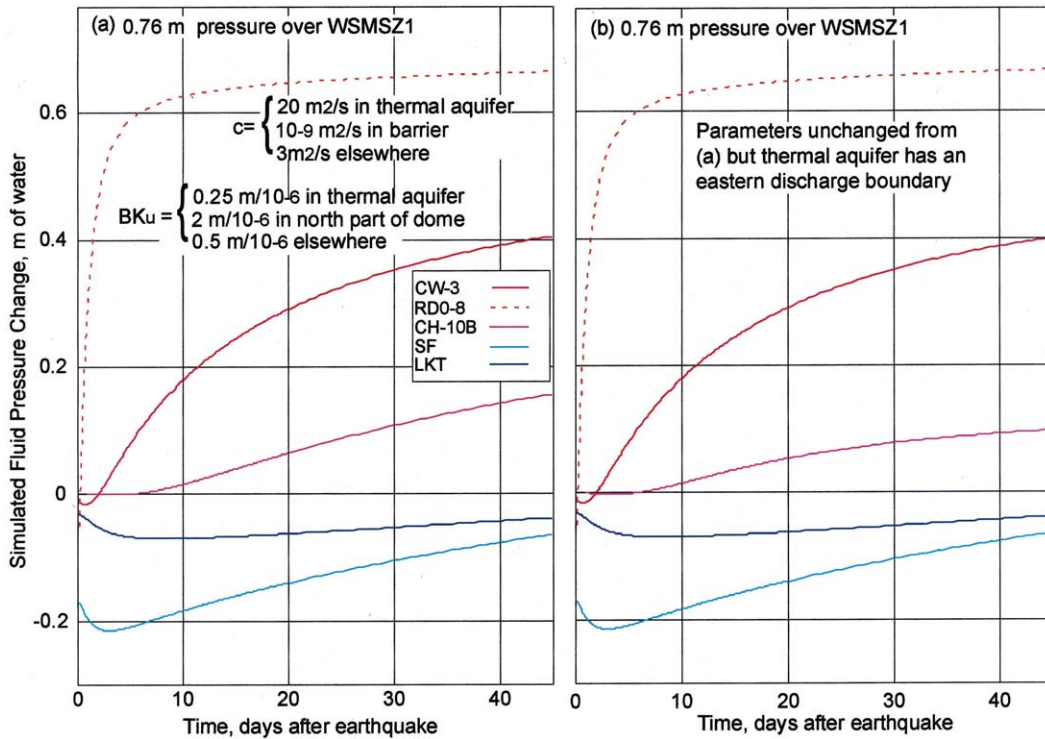


Fig. 17. Simulated time histories of fluid pressure at observation wells with addition of fixed 0.76 m pressure above WSMSZ1 and a flow barrier at the northern edge of the thermal aquifer. (a) Simulation as in Fig. 16b, but with diffusivity of thermal aquifer adjusted upward to match time history at CW-3. (b) Effect of introducing a zero-pressure boundary at eastern edge of thermal aquifer.

could confirm or disprove fluid-pressure increases over WSMSZ1, since a rapid water-level rise nearly equal to the assumed pressure pulse is simulated there (Fig. 17b). At the time of the 1992 Landers earthquake, water level in the RDO-8 well was dropping due to a temporary cessation of injection in the geothermal field. When the earthquake occurred, water level at RDO-8 oscillated and then rapidly dropped 12 cm; it began to rise 2 days later, but this could have been caused by the resumption of geothermal fluid injection (Roeloffs et al., 1995). At least for the Landers earthquake, a large, rapid water-level rise at RDO-8 did not occur. Only manual measurements are available for RDO-8 in 1997; they permit a maximum net water-level rise of 0.3 m during the November–December 1997 activity.

The fluid-pressure increase could, alternatively, take place further east, closer to CW-3. If increased pressure occurs above the plane SERD1

(Fig. 15) identified by Prejean et al. (2002), which is in the approximate location of ‘Fumarole Valley’ (Fig. 2), the time history at CW-3 can be well matched using a much lower diffusivity ($0.01 \text{ m}^2 \text{ s}^{-1}$) and smaller amplitude of pressure increase (53 cm of water; Fig. 18). The diffusive delay is short enough to agree with the data and no change is predicted at CH-10B. On the other hand, the 12-h ramp time history with which the pressure is imposed is evident in the response at CW-3; if SERD1 is the appropriate location for the increased pressure then it must have a smoother onset. A source above SERD1 would not increase the water-level at RDO-8. Models placing pressure sources at intermediate locations in the south moat could also match the CW-3 data with intermediate values of the hydraulic diffusivity. Only if the location were better known could the rise time of the pressure source be constrained.

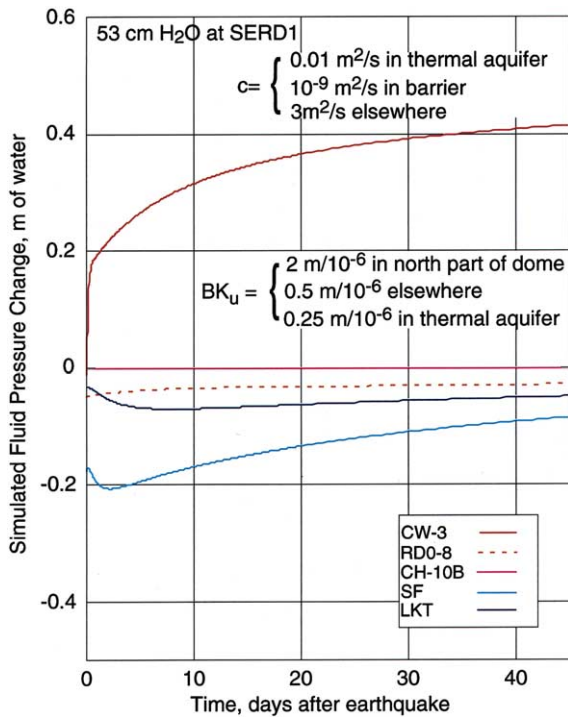


Fig. 18. Simulated time histories for thermal pressure at SERD1.

Increased pressure of 50–100 cm of water is needed to match the CW-3 observations. The maximum pressure rise adjacent to an intrusion, Δp , is given by Delaney (1982) as:

$$\Delta p = \alpha \Delta T \sqrt{\kappa/c} / \beta \quad (6)$$

In Eq. 6, α is the coefficient of isobaric volumetric thermal expansion for the fluid (neglecting thermal expansion of the matrix and grains), ΔT is the temperature rise, κ is thermal diffusivity ($10^{-6} \text{ m}^2 \text{ s}^{-1}$), and β is the isothermal volumetric compressibility, computed from the compressibilities of the solid and the fluid and the porosity. α and the fluid compressibility both depend on pressure and temperature. The ‘overall expansion’ $\alpha \Delta T$ is plotted in fig. 4b of Delaney (1982); typical values are 0.6 for $\Delta T = 300^\circ\text{C}$ to a maximum of 0.8–1.0 for $\Delta T = 400^\circ\text{C}$ to 1000°C . $\sqrt{\kappa/c}$ is the ratio of penetration depth of the thermal disturbance to that of the fluid-pressure disturbance; for diffusivities of $0.01\text{--}20 \text{ m}^2 \text{ s}^{-1}$, $\sqrt{\kappa/c}$ ranges

from 2.2×10^{-4} to 0.01. Finally, β is in the range of $0.02\text{--}2 \text{ GPa}^{-1}$. Using the higher compressibilities and lower values of $\sqrt{\kappa/c}$ in Eq. 6 yields a minimum $\Delta p = \alpha \Delta T \times 0.11 \text{ MPa}$, equivalent to 6.6 m of water for $\Delta T = 300^\circ\text{C}$ or 9–11 m of water for a temperature rise of $\Delta T = 400^\circ\text{C}$ or more. Thus, for diffusivities appropriate to the upper 1000 m at Long Valley caldera, pressure increases adjacent to intruded hot material can be an order of magnitude larger than those required in the thermal aquifer to account for the earthquake-induced water-level rises at CW-3.

The water-level data contain no information about the shallowest depth to which hot material could have penetrated, or whether that material would be molten rock or hot aqueous fluid. The minimum depth of seismicity in November 1997 was 0.5 km, near the lower limit of the shallow thermal aquifer. If hot material came this close to the surface, then vertical diffusion of pressure would add little delay to the time required for elevated pressure to be observed in CW-3, which is 300 m deep. Most seismic activity is 3.5 km deep or more, however. A localized zone of high vertical diffusivity would be required to transmit thermal pressure from this depth to CW-3 without observable delay.

5.4. November 1997

The water-level changes that began abruptly following the M4.9 earthquake on November 22, 1997, at 17:20 UT are unique in that deformation was observed on the two-color EDM network during the succeeding several days while the gradual water-level changes were taking place. Distinct coseismic steps at the wells (expressed in units of strain) and the POP strainmeter can be used to investigate whether opening-mode displacement occurred in the south moat during the hour following this earthquake. The water-level and strain data provide only four points to constrain a dislocation model; the only additional requirement is to avoid violating the two-color EDM data. This limited data set does, however, permit discrimination among models consisting of right-lateral and/or opening-mode slip on two rectangular slip planes: the approximate fault plane of the 17:20

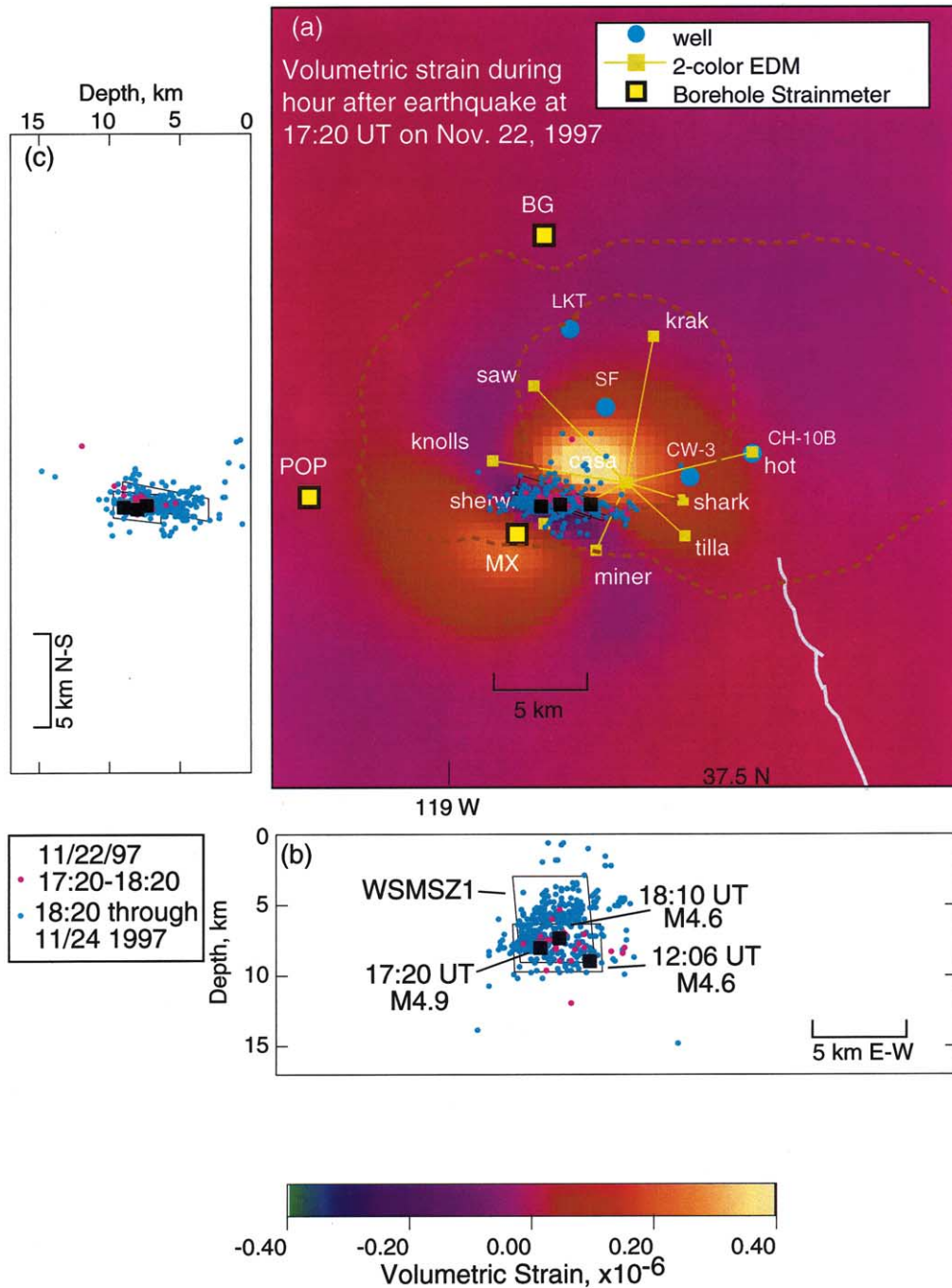


Fig. 19. (a) Map showing epicenters of earthquakes during the period November 22, 1997, 17:20 UT through November 24, 1997. Surface projections of fault plane of earthquake at 17:20 UT and of plane WSMSZ1 are also shown. Contours are volumetric strain calculated from dislocation model fit to observed strain in the first hour after 17:20. (b) East–west cross-sectional view of seismicity and planes. (c) North–south cross-sectional view of seismicity and planes.

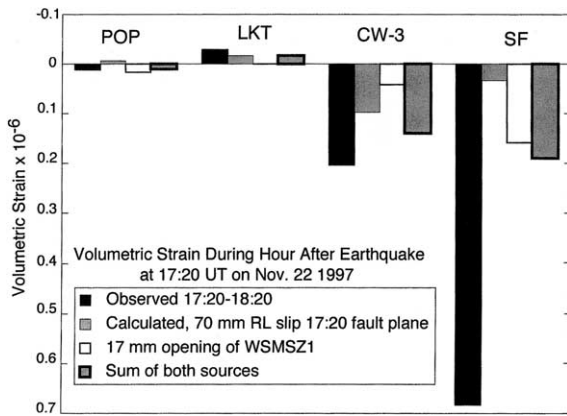


Fig. 20. Contributions of right-lateral slip over the fault plane of the earthquake at 17:20 UT and opening of plane WSMSZ1 to calculated strain at observation wells and POP strainmeter, compared with observed strain in the hour following the 17:20 earthquake.

earthquake, and the plane WSMSZ1 of [Prejean et al. \(2002\)](#) over which seismicity propagated upward ([Fig. 19](#)). We reject models that change any of the frequently measured two-color EDM lines by more than 1 mm.

No model in this class fully accounts for the large extension at SF ([Fig. 20](#)). If displacement during the first hour after 17:20 UT is restricted to the relatively deep fault plane containing the seismicity during that period, then 80–100 mm of right-lateral slip account for the steps at CW-3 and LKT, but produce only 0.05×10^{-6} extension at SF, and also imply contraction rather than extension at POP. Opening-mode displacement restricted to this deep plane does not significantly improve the fit. The addition of opening-mode slip over WSMSZ1 does improve the fit by producing more extension at SF and extension at POP. The data points cannot discriminate between right-lateral slip over the 17:20 fault plane and right-lateral slip over WSMSZ1, which overlap. A combined model including 70-mm right-lateral slip over the 17:20 fault plane and 17-mm opening of WSMSZ1 ([Fig. 20](#)) provides an acceptable fit to the data, although the contraction at LKT is still underpredicted by 15% and only $0.15\text{--}0.25 \times 10^{-6}$ extension at SF are accounted for. Since seismicity actually occurred at depths shallower than the top of WSMSZ1 (3.0

km), we tested additional models with opening-mode displacement on the up-dip extension of WSMSZ1, but rejected them because they produce substantially less extension at SF. We conclude that deformation over the plane of the 17:20 event and/or WSMSZ1 cannot account for the large observed extension at SF. Inflation of the dome would produce large extension at SF, but does not improve the fit to the coseismic steps because such inflation also produces extension at LKT, which was not observed. If dome inflation occurred, then it took place more slowly than during the hour following the 17:20 earthquake.

The strain field throughout Long Valley caldera that would be produced by the combined model (70-mm right-lateral slip over the 17:20 fault plane and 17-mm opening of WSMSZ1) imposes extension on the dome in the same area as point or ellipsoidal inflation sources ([Fig. 19](#)). Primarily for this reason, simulated diffusional decay of undrained fluid pressure calculated from the strain shown in [Fig. 19](#) is very similar to that calculated assuming only a dome inflation source.

Interestingly, the combined model also produces extension in the vicinity of Mammoth Mountain. Qualitatively, such extension would produce a zone of lower fluid pressure that could diffuse to the location of POP, creating contractional strain. The amplitude of the extension in [Fig. 19](#) is probably insufficient, however, to account for the strain changes observed in November 1997.

6. Concluding discussion

Water-level changes in Long Valley induced by earthquakes can be accounted for by accelerated inflation of the resurgent dome plus localized fluid-pressure increases due to thermal pressurization in the south moat. A two-dimensional model of groundwater flow in response to these effects successfully explains the time histories of the water-level changes at LKT, but underestimates the sizes of many of them, which we believe could be resolved using a more detailed model.

The earthquake-induced water-level rises at CW-3 are closely modeled as diffusive responses to localized pressure increases in the south moat.

Because contractional strain sufficient to cause such a rise is incompatible with the two-color EDM data, we propose that these localized pressure increases are caused by thermal pressurization that is in turn due to upward movement of hot material, either magma or aqueous fluid, beneath the south moat. The rapid onset of increased pressure at CW-3 is most easily explained if the hot material has risen to within 1 km of the surface at a location within 1 km of CW-3. Discharge increases at the Hot Creek Flume and Little Hot Creek (Fig. 2) at the times of $M \geq 6$ earthquakes near Long Valley support the idea that earthquakes tend to raise pressure in the thermal aquifer (Sorey and Clark, 1991). Additional wells exist in the south moat that could constrain the possible location of thermal-pressure increases, although data are currently proprietary. Temperature variations with time in the thermal aquifer might be difficult to associate with individual episodes because their penetration distances are two to four orders of magnitude smaller than those of the induced pressure disturbances.

The contractional signals at the POP strainmeter remain unexplained. These signals are too large to be accounted for by sources in the caldera at shallow depth, and likely require a somewhat independent process occurring locally near POP.

In the model proposed here, shallow fluid diffusion dominates the time histories of earthquake-induced water-level changes at LKT and CW-3, masking the time dependence of postulated earthquake-triggered deformation or thermal-pressure increases. For the water-level changes following distant earthquakes, the absence of steps does suggest that the deformation requires at least hours to occur. On the other hand, the time-dependence of the water-level and strain changes could alternatively be explained by sources that change in intensity and geometry with time.

Water-level changes at Long Valley that are induced by distant earthquakes have some features in common with the same phenomenon at other locations where triggering of aseismic deformation or volcanic activity can be ruled out. This study implies that seismic waves can produce water-level changes in several different ways, because for Long Valley the evidence is strong that

these changes actually reflect earthquake-induced accelerated volcanic deformation.

Seismic-wave-induced processes at Long Valley must represent the behavior of hydrothermal or volcanic features. Although seismic waves from distant earthquakes are capable of causing long-lasting fluid-pressure changes in many locations, borehole strain recordings show that step-like strain changes, transient strain episodes, or strain-rate changes are not generally produced by seismic waves. Additional evidence suggests that seismic waves from distant earthquakes have their most significant effects in hydrothermal areas. Most of the locations in the western United States where the Landers and Hector Mine earthquakes triggered microseismicity were geothermal areas (Hill et al., 1993; Gombert et al., 2001). Brodsky et al. (2000) identified microseismicity in Greece triggered by the August 1999 Izmit, Turkey, earthquake, much of it in areas with thermal springs. Johnson et al. (2001) showed that earthquakes over 200 km distant could increase temperatures measured in the discharge vents of hydrothermal springs on the Juan de Fuca ridge.

Features at Long Valley that might be preferentially affected by seismic waves include fluid-filled fissures at low effective stress, recently active faults, magma in subsurface reservoirs, dikes, or pipes, and young seals in hydrothermal systems. Hot magmatic fluids in the subsurface alter and weaken the rocks at their edges. These weakened rocks could be loosened or cracked by dynamic strains, clearing pathways for fluid movement. Others have proposed that seismic waves can affect fluid pressures by rectified diffusion (Sturtevant et al., 1996), rising of bubbles (Linde et al., 1994), or by flashing of superheated fluid to steam. This study provides observational evidence that seismic waves can stimulate hydrothermal systems, that such stimulation is likely related to remote triggering of earthquakes, and that the processes involved can be illuminated by hydrologic monitoring in active volcanic areas.

Acknowledgements

We are grateful to R. Jacobson of Sandia Na-

tional Laboratories for generously making available the pressure data recorded in the LVEW during the Hector Mine earthquake. We thank S. Prejean for her relative earthquake relocations and for many stimulating discussions about their significance. Comments by S. Hurwitz, C. Wicks, and E. Brodsky were valuable in improving the manuscript. We used earthquake data from the CNSS, the Berkeley Seismological Laboratory, and the USGS Menlo Park Northern California Seismic Network, obtained from the Northern California Earthquake Data Center.

References

- Aoki, Y., Segall, P., Kato, T., Cervelli, P., Shimada, S., 1999. Imaging magma transport during the 1997 seismic swarm off the Izu peninsula, Japan. *Science* 286, 927–930.
- Bailey, R.A., 1989. Geologic Map of Long Valley caldera, Mono-Inyo Craters Volcanic Chain and Vicinity, Eastern California. U.S. Geol. Surv. Map I-1933, 2 sheets, 11 pp.
- Bailey, R.A., Hill, D.P., 1990. Magmatic unrest at Long Valley caldera, California, 1980–1990. *Geosci. Can.* 17, 175–178.
- Blackwell, D.D., 1985. A transient model of the geothermal system of the Long Valley caldera, California. *J. Geophys. Res.* 90, 11229–11242.
- Brodsky, E.E., Karakostas, V., Kanamori, H., 2000. A new observation of dynamically triggered regional seismicity: Earthquakes in Greece following the August, 1999 Izmit, Turkey earthquake. *Geophys. Res. Lett.* 27, 2741–2744.
- Brodsky, E.E., Roeloffs, E., Woodcock, D., Gall, I., Manga, M., 2003. A mechanism for sustained groundwater pressure changes induced by distant earthquakes. *J. Geophys. Res.*, in press.
- Bullen, K.E., Bolt, B.A., 1985. *An Introduction to the Theory of Seismology*. Cambridge University Press, Cambridge, 499 pp.
- Delaney, P.T., 1982. Rapid intrusion of magma into wet rock: Groundwater flow due to pore pressure increases. *J. Geophys. Res.* 87, 7739–7756.
- Dreger, D.S., Tkalic, H., Johnston, M., 2000. Dilational processes accompanying earthquakes in the Long Valley caldera. *Science* 288, 122–125.
- Galloway, D.L., Farrar, C.D., Howle, J.F., Roeloffs, E.A., Sneed, M., Sorey, M.L., 1999. Hydrologic response to the 1997–98 period of crustal unrest at Long Valley caldera, California (abstract). *Suppl. EOS Trans. Am. Geophys. Union* 80, F981.
- Gomberg, J., Reasenber, P., Bodin, P., Harris, R., 2001. Earthquake triggering by transient seismic waves following the Landers and Hector Mine, California earthquakes. *Nature* 411, 462–466.
- Hill, D.P., Reasenber, P.A., Michael, A., Arabasz, W.J., Be-roza, G., Brumbaugh, D., Brune, J.N., Castro, R., Davis, S., dePolo, D., Ellsworth, W.L., Gomberg, J., Harmsen, S., House, L., Jackson, S.M., Johnston, M.J.S., Jones, L., Keller, R., Malone, S., Munguia, L., Nava, S., Pechmann, J.C., Sanford, A., Simpson, R.W., Smith, R.B., Stark, M., Stickney, M., Vidal, A., Walter, S., Wong, V., Zollweg, J., 1993. Seismicity in the western United States remotely triggered by the magnitude 7.3 Landers, California earthquake. *Science* 260, 1617–1623.
- Hill, D.P., Johnston, M.J.S., Langbein, J.O., Bilham, R., 1995. Response of Long Valley Caldera to the Mw 7.3 Landers, California earthquake. *J. Geophys. Res.* 100, 12985–13005.
- Hill, D.P., Dzurisin, D., Ellsworth, W.L., Endo, E.T., Galloway, D.L., Gerlach, T.M., Johnston, M.J.S., Langbein, J.O., McGee, K.A., Miller, C.D., Oppenheimer, D., Sorey, M.L., 2002. Response Plan for Volcano Hazards in the Long Valley Caldera and Mono Craters Region, California. U.S. Geol. Surv. Bull. 2185, 57 pp.
- Howle, J.F., Farrar, C.D., 1996. Hydrologic Data for Long Valley Caldera, Mono County, California, 1987–1993. U.S. Geol. Surv. Open-File Rep. 96-382, 286 pp.
- Johnson, H.P., Dziak, R.P., Fisher, C.R., Fox, C.G., Pruis, M.J., 2001. Earthquakes' impact on hydrothermal systems may be far-reaching. *EOS Trans. Am. Geophys. Union* 82, 233–236.
- Johnston, M.J.S., Hill, D.P., Linde, A.T., Langbein, J., Bilham, R., 1995. Transient deformation during triggered seismicity from the 28 June 1992 $M_w = 7.3$ Landers earthquake at Long Valley Volcanic Caldera, California. *Bull. Seismol. Soc. Am.* 85, 787–795.
- Koizumi, N., Tsukuda, E., Kamigaichi, O., Matsumoto, N., Takahashi, M., Sato, T., 1999. Preseismic changes in groundwater level and volumetric strain associated with earthquake swarms off the east coast of Izu Peninsula, Japan. *Geophys. Res. Lett.* 26, 3509–3512.
- Langbein, J., Hill, D.P., Parker, T.N., Wilkinson, S.K., 1993. An episode of reinflation of the Long Valley caldera, eastern California: 1989–1991. *J. Geophys. Res.* 98, 15851–15870.
- Langbein, J., Dzurisin, D., Marshall, G., Stein, R., Rundle, J., 1995. Shallow and peripheral volcanic sources of inflation revealed by modeling two-color geodimeter and leveling data from Long Valley caldera, California, 1988–1992. *J. Geophys. Res.* 100, 12487–12495.
- Langbein, J.O., 2003. Deformation of the Long Valley caldera, California: inferences from measurements from 1988 to 2001. *J. Volcanol. Geotherm. Res.* 127, 247–267.
- Linde, A.T., Sacks, I.S., Johnston, M.J.S., Hill, D.P., Bilham, R.G., 1994. Increased pressure from rising bubbles as a mechanism for remotely triggered seismicity. *Nature* 371, 408–410.
- Matsumoto, K., Takanezawa, T., Ooe, M., 2000. Tide models developed by assimilating TOPEX/POSEIDON altimeter data into hydrodynamical model: A global model and a regional model around Japan. *J. Oceanogr.* 56, 567–581.
- Matsumoto, N., 1992. Regression analysis for anomalous

- changes of ground water level due to earthquakes. *Geophys. Res. Lett.* 19, 1193–1196.
- Matsumoto, N., Roeloffs, E.A., 2003. Hydrologic response to earthquakes in the Haibara well, central Japan: II. Possible mechanism inferred from time-varying hydraulic properties. Submitted to *Geophys. J. Int.*
- McConnell, V.S., Shearer, C.K., Eichelberger, J.C., Keskinen, M.J., Layer, P.W., Papike, J.J., 1995. Rhyolitic intrusions in the intracaldera Bishop Tuff, Long Valley Caldera, California. *J. Volcanol. Geotherm. Res.* 67, 41–60.
- Okada, Y., 1992. Internal deformation due to shear and tensile faults in a half-space. *Bull. Seismol. Soc. Am.* 82, 1018–1040.
- Okada, Y., Yamamoto, E., 1991. Dyke intrusion model for the 1989 seismovolcanic activity off Ito, central Japan. *J. Geophys. Res.* 96, 10361–10376.
- Prejean, S., Ellsworth, W., Zoback, M., Waldhauser, F., 2002. Fault structure and kinematics of the Long Valley Caldera region, California, revealed by high-accuracy earthquake hypocenters and focal mechanism stress inversions. *J. Geophys. Res.*, 107, ESE 9-1 to ESE 9-19.
- Prejean, S., 2002. The Interaction of Tectonic and Magmatic Processes in the Long Valley Caldera, California. Ph.D. Thesis, Stanford University, Stanford, CA, 145 pp.
- Roeloffs, E.A., 1996. Poroelastic methods in the study of earthquake-related hydrologic phenomena. In: Dmowska, R. (Ed.), *Advances in Geophysics*. Academic Press, San Diego, CA, pp. 135–195.
- Roeloffs, E., 1998. Persistent water level changes in a well near Parkfield, California, due to local and distant earthquakes. *J. Geophys. Res.* 103, 869–889.
- Roeloffs, E.A., Danskin, W.R., Farrar, C.D., Galloway, D.L., Hamlin, S.N., Quilty, E.G., Quinn, H.M., Schaefer, D.H., Sorey, M.L., Woodcock, D.E., 1995. Hydrologic Effects Associated with the June 28, 1992 Landers, California, Earthquake Sequence. U.S. Geol. Surv. Open-File Rep. 95-42, 68 pp.
- Rojstaczer, S., 1988. Intermediate period response of water levels in wells to crustal strain: sensitivity and noise level. *J. Geophys. Res.* 93, 13619–13634.
- Rojstaczer, S., Agnew, D.C., 1989. The influence of formation material properties on the response of water levels in wells to earth tides and atmospheric loading. *J. Geophys. Res.* 94, 12403–12411.
- Sato, T., Hanada, H., 1984. A program for the computation of oceanic tidal loading effects 'GOTIC'. *Publ. Int. Latit. Obs. Mizusawa* 18, 29–47.
- Sorey, M.L., 1985. Evolution and present state of the hydrothermal system in Long Valley caldera. *J. Geophys. Res.* 90, 11219–11228.
- Sorey, M.L., Lewis, R.E., Olmsted, F.H., 1978. The Hydrothermal System of Long Valley Caldera, California. U.S. Geol. Surv. Prof. Pap. 1044-A, 60 pp.
- Sorey, M.L., Clark, M.D., 1991. Changes in the Discharge Characteristics of Thermal Springs and Fumaroles in the Long Valley Caldera, California, Resulting from Earthquakes on May 25–27, 1980. U.S. Geol. Surv. Open-File Rep. 81-0203, 25 pp.
- Sorey, M.L., Suemnicht, G.A., Sturchio, N.C., Nordquist, G.A., 1991. New evidence on the hydrothermal system in Long Valley caldera, California, from wells, fluid sampling, electrical geophysics, and age determinations of hot-spring deposits. *J. Volcanol. Geotherm. Res.* 48, 229–263.
- Sorey, M.L., Farrar, C.D., 1998. Changes in surficial features associated with geothermal development in Long Valley caldera, California, 1985–1997. *Geotherm. Resour. Council Trans.* 22, 61–63.
- Sturtevant, B., Kanamori, H., Brodsky, E.E., 1996. Seismic triggering by rectified diffusion in geothermal systems. *J. Geophys. Res.* 101, 25269–25282.